Journal of the European Ceramic Society xxx (xxxx) xxx

Contents lists available at ScienceDirect

Journal of the European Ceramic Society

journal homepage: www.elsevier.com/locate/jeurceramsoc

Review article

Silica-based ceramics toward electromagnetic microwave absorption

Xiaojun Zeng [a,b,*,1], Eugene Li [b,1], Guohua Xia [a], Nuohua Xie [a], Zong-Yang Shen [a,*], Martin Moskovits [b], Ronghai Yu [c]

[a] China National Light Industry Key Laboratory of Functional Ceramic Materials, School of Materials Science and Engineering, Jingdezhen Ceramic University, Jingdezhen, 333403, China
[b] Department of Chemistry and Biochemistry, University of California Santa Barbara, Santa Barbara, CA, 93106, United States
[c] School of Materials Science and Engineering, Beihang University, Beijing, 100191, China

ARTICLE INFO

Keywords:
Silica-based ceramics
Composite ceramics
Electromagnetic microwave absorption
Structure design
Reflection loss

ABSTRACT

Silica-based ceramics have been explored extensively as a class of versatile materials for various applications in architecture, catalysis, energy, machinery, and biomedical engineering. Nevertheless, comprehensive information on silica-based ceramic and electromagnetic microwave (EMW) absorption is scarce, although excellent progress has been made in this field. Here, recent progress in the investigation of silica-based ceramics toward EMW absorption is reviewed. We first introduced the basis of ceramics (characteristics, classification, synthetic methods, potential applications). Subsequently, the silica-based ceramics, including Si-based oxides and alloys, SiOC/SiC/Si_3N_4/SiCN-based composite, Ti_3SiC_2 and composite for EMW absorption were systematically summarized. Notably, the fabrication strategies, absorption properties, and mechanisms of silica-based ceramics are described in detail, with a focus on structure and component design. Lastly, the prospects and ongoing challenges of this field in the future are presented. This review is expected to learn from the past and achieve progress toward the future of silica-based ceramic for EMW absorption.

1. Introduction

The increasingly fierce international military competition has promoted the rapid development of various high-technology military weapons and equipment, especially stealth fighters and unmanned aerial vehicles, which also puts forward a new perspective on the development and research of corresponding electromagnetic microwave (EMW) absorbing and shielding materials [1–4]. Meantime, the promotion of 5 G accelerates the digital transformation and product upgrades, which makes the interference of related digital equipment more serious, and the emitted electromagnetic radiation has also caused greater harm to human health [5–8]. Therefore, solving the problems of electronic equipment interference, electromagnetic radiation hazards, and fighter stealth is an attractive and challenging topic. In the end, various types of electromagnetic microwave (EMW) absorbing and shielding materials including carbon-based materials (CNTs, graphene, carbon fiber, graphitized carbon, polymer) [9–12], metal compounds (oxide, sulfide, nitride, carbide) [13–16], metal-organic framework (MOF) [17–19], MXene [20–23], and composite materials [24–27] have been developed to enable considerable EMW absorption performance with high reflection loss (R_L), wide effective absorption bandwidth ($R_L <$ -10 dB), thin thickness, and low density.

Generally, EMW absorption materials mainly use magnetic loss, dielectric loss (especially polarization, such as electronic polarization and interface polarization), and other mechanisms to achieve EMW absorption ability [28,29]. Although the early-developed EMW absorption materials have made gratifying progress in magnetic or dielectric loss, their relatively high density, low reflection loss, and narrow effective absorption bandwidth have relatively hindered their application breadth, speed, and scale of production development [30,31]. Among them, ceramic materials, especially silica-based ceramics, have elicited considerable attention in the EMW absorption field since the advantages of high thermal and chemical stability, remarkable mechanical strength and hardness, low prices, abundant reserves, and large-scale preparation [32–35]. However, the large-scale application of silica-based ceramic EMW absorbers is hindered predominantly by their

* Corresponding authors at: China National Light Industry Key Laboratory of Functional Ceramic Materials, School of Materials Science and Engineering, Jingdezhen Ceramic University, Jingdezhen, 333403, China.
E-mail addresses: zengxiaojun@jci.edu.cn (X. Zeng), shenzongyang@163.com (Z.-Y. Shen).
[1] These authors contributed equally to this work.

https://doi.org/10.1016/j.jeurceramsoc.2021.08.009
Received 18 June 2021; Received in revised form 2 August 2021; Accepted 6 August 2021
Available online 12 August 2021

large weight, dense structure, and high heat-treatment temperature. Therefore, the design and exploration of high-performing silica-based ceramic EMW absorbers is a critical objective. Some of these explorations are based on uniquely designed novel nanostructures, which give them the ability to scatter and reflect electromagnetic waves multiple times and increase the transmission path of electromagnetic waves [36–39]. Other explorations are based on component design to deliver materials with good impedance matching between magnetic loss and dielectric loss [40–44]. Nevertheless, comprehensive information including the fabrication strategies, EMW absorption performance, and EMW absorption mechanisms on silica-based ceramic in the field of EMW absorption is scarce, although it has made such excellent progress in this field.

Although silica-based ceramics applied in EMW absorption have been studied for many years, the increasing researches on this field indicated the unique advantages of silica-based ceramics as EMW absorption materials, opening a new chapter between silica-based ceramics and EMW absorption. This timely review aims to afford readers a deep insight into the development of silica-based ceramics for EMW absorption. In this review, we will briefly introduce the definition and characteristics, classification, synthetic methods, and potential applications of ceramics, summarize the silica-based ceramic materials used for EMW absorption, and highlight their fabrication strategies, EMW absorption properties, and corresponding EMW absorption mechanisms. Finally, the future outlooks and our viewpoints on this research topic are presented. We hope that our work can promote the development of silica-based ceramics in the field of EMW absorption to achieve more significant breakthroughs.

2. Basis of ceramics

2.1. Definition and characteristics of ceramics

Ceramics are non-metallic inorganic materials with a wide range of components [45], which together with metals and polymers become structural materials [46]. The American Society for Testing and Materials defines a ceramic material as “an article [whose] body is produced from essentially inorganic, non-metallic substances and either is formed from a molten mass which solidifies on cooling, or is formed and simultaneously or subsequently matured by the action of the heat.” [47]. Meanwhile, Kingery defines ceramics as “the art and science of making and using solid articles which have as their essential component, and are composed in large part of, inorganic non-metallic materials” [48]. Although metals are stronger, cheaper, and tougher, they are chemically active, heavy, and have limited operating temperatures [46,49–53]. Polymers are highly flexible, easy to manufacture, and light in weight, but they can only be used at very low temperatures [54–59]. Compared with metals and polymers, the main characteristics of ceramic materials include insulation, corrosion resistance, high-temperature resistance, high hardness, superior wear resistance, radiation resistance, thermal shock resistance, lower thermal and electrical conductivity [32–35]. The typical performance evaluation index of colorful ceramics including density and cost (moderate to high), thermal conductivity (low to high), synthesis temperature (high, < 1650 ℃), chemical resistance (excellent), mechanical properties (good), and main weaknesses (Inherent brittleness) [47].

However, most ceramics are porous and brittle. Ceramic materials are composed of ionic bonds or covalent bonds, and their structure is crystalline or amorphous [47]. This electronic bonding makes ceramics prone to fracture rather than undergoing plastic deformation, so their tensile strength and toughness are low. Furthermore, ceramic materials are usually porous, and microscopic pores are known to act as stress concentrators, which will further reduce the strength and toughness of the ceramic. The aforementioned defects lead to the catastrophic failure of the ceramic materials, and resulting in low damage tolerance of the component under service conditions [60]. Although easily overlooked, ceramic materials do undergo plastic deformation. In crystalline ceramic materials, due to the rigid structure of ceramics and the lack of a slip system for dislocation movement, this deformation process occurs very slowly. For non-crystalline ceramic materials, viscous flow is the dominant source of plastic deformation, and the speed is also very slow.

2.2. Classification of ceramics

Ceramics have a history of nearly ten thousand years, which currently provide us with a wide variety of materials [61] (Fig. 1). Ceramics can be roughly divided into glass, glass ceramics, and engineering ceramics, among which engineering ceramics mainly include traditional ceramics and special/fine ceramics. Traditional ceramics [62,63], including daily-use ceramics, building and sanitary ceramics, arts and crafts ceramics, chemical ceramics, electrical ceramics, etc. These are primarily made of natural silicates, such as clay ($Al_2O_3{\cdot}2SiO_2{\cdot}2H_2O$), quartz ($SiO_2$), feldspar ($K_2O{\cdot}Al_2O_3{\cdot}6SiO_2$ or $Na_2O{\cdot}Al_2O_3{\cdot}6SiO_2$), or kaolin ($Al_2O_3{\cdot}2SiO_2{\cdot}2H_2O$). Traditional ceramics are generally hard, brittle, insulating materials that possess high-temperature resistance, high hardness, radiation resistance, and brittleness. Later special/fine ceramics are divided into structural ceramics and functional ceramics [64–66], such as piezoelectric ceramics, magnetic ceramics, capacitor ceramics, and high-temperature ceramics (oxide ceramics, carbide ceramics, nitride ceramics, and boride ceramics). Compared with traditional ceramics, special/fine ceramics have higher temperature resistance, mechanical properties, special electrical properties, and excellent chemical resistance.

2.3. Synthetic methods of ceramics

The richness and functionality of ceramics have prompted researchers to continuously develop various technologies to synthesize advanced ceramic materials (Fig. 2) [67]. Generally, the preparation process of ceramics is to first mix the ceramic raw material particles, water, and/or organic binder uniformly in a certain proportion [48,68], and then mold the resulting mixture to obtain the desired size and shape. After drying and evaporating the water, the ceramic is finally densified by heat treatment and given certain mechanical strength and hardness. It is conceivable that the final microstructure and mechanical properties of ceramics depend to a large extent on the molding process and sintering process, especially the maximum temperature and duration of the heat treatment.

Ceramic molding technology primarily includes grouting molding, tap casting, freeze casting, hot die casting, plastic molding (rolling molding, extrusion molding, injection molding, plastic compression molding, rolling film molding), compression molding (dry pressing molding, semi-dry pressing molding, isostatic pressing molding), fused deposition molding, three-dimensional (3D) printing, inkjet printing, and stereolithography molding, etc. [69–75]. Inkjet printing is a material-conserving deposition technique for liquid-phase materials [76]. This technology mainly involves the ejection of a fixed amount of ink in a chamber, from a nozzle through a sudden, quasi-adiabatic reduction of the chamber volume via piezoelectric action. Stereolithography is a rapid prototyping technology based on photopolymerization, involving computer-driven and spatially controlled irradiation of liquid resin [77]. This method can directly prepare structures with precise microscale features from computer models. Traditional ceramic molding takes a long time, is costly, and cannot produce highly complex shapes of ceramics. The extremely high hardness and brittleness of ceramic parts have other shortcomings. They are extremely difficult to process. Defects such as cracks are easily formed during processing, making it difficult to obtain good surface quality and precise dimensions [73]. Technologies such as 3D printing, inkjet printing, and stereolithography molding developed in recent years have addressed these shortcomings.

The sintering process (Fig. 2), including densification and grain

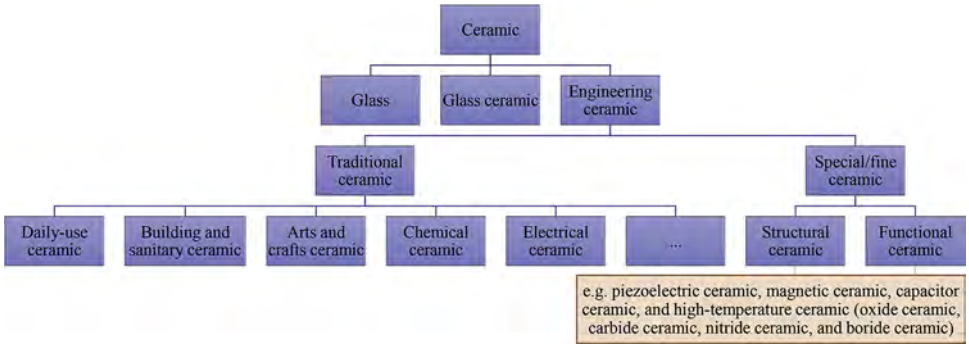

Fig. 1. Scheme showing the classification of ceramics.

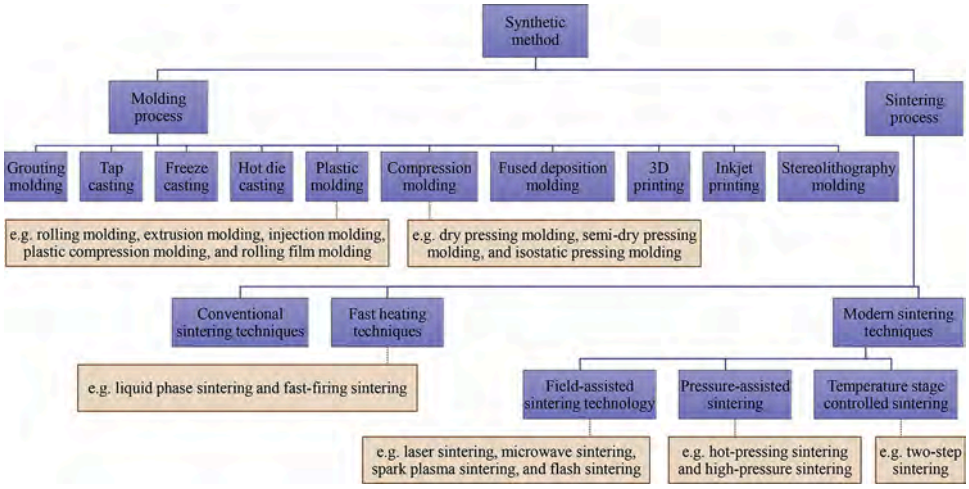

Fig. 2. Scheme showing the molding process and sintering process of ceramics.

growth, of ceramics, will directly affect the grain size, microstructure, and porosity of the ceramics, and then determine the final properties of the ceramics. Compared with conventional sintering techniques, fast heating techniques (e.g., liquid phase sintering, fast-firing sintering) and modern sintering techniques [78,79], such as field-assisted sintering technology (e.g., laser sintering, microwave sintering, spark plasma sintering, and flash sintering) [80,81], pressure-assisted sintering (e.g., hot-pressing sintering, high-pressure sintering) and temperature stage controlled sintering (e.g., two-step sintering) [82], can further promote the densification of grain growth. Consequently, the sintering temperature and time can be significantly reduced, so that energy consumption is relatively low. Newly developed advanced sintering techniques (e.g., cold sintering developed at The Pennsylvania State University, ultrafast high-temperature sintering reported by Hu and co-workers) enable other advantages in this respect [83–89].

2.4. Potential applications of ceramics

Ceram enables high thermal and chemical stability, remarkable mechanical strength and hardness, and large optical, electrical, and magnetic performance, making it a multifunctional application material, such as architecture [90,91], catalysis (heterogeneous catalysis, electrocatalysis, and photocatalysis) [92–97], energy (solar cells, batteries, fuel cells, and supercapacitor) [98–106], machinery, electronics [107], chemical industry [108], biomedical engineering [109], and aerospace [110]. With the improvement of synthesis technology, various ceramic materials with novel structures have been continuously prepared, which makes their applications more abundant. For example, many advanced ceramics have been developed recently, such as ceramic aerogels for thermal superinsulation [111], long-term heat-storage ceramics (λ-$Sc_xTi_{3-x}O_5$) [112], foam ceramics (Al_2O_3) with near-zero sintering shrinkage [113], lamellar ceramic sponges for acoustic absorption [114], super-strong and elastic ceramics [115], photothermal conversion ceramics (MXene) [116], and polymer derived ceramics for microwave absorption [117].

3. Silica-based ceramics toward EMW

Nevertheless, ceramic materials have specific applications in various fields, but their applications in the field of electromagnetic microwave (EMW) absorption are considerably important. The main reason is that electromagnetic (EM) radiation generated by constantly updated digital devices (such as mobile phones, computers, and airplanes) has caused great harm to human health. These challenges have prompted researchers to develop advanced materials for absorbing EMW. Among them, the development of silica-based ceramic materials including Si-based oxides and alloys ceramics, SiOC-based composite ceramics, SiC-based composite ceramics, Si_3N_4-based composite ceramics, SiCN-based composite ceramics, Ti_3SiC_2 and composite ceramics is no exception. This can be attributed to the advantages of silica-based ceramics such as high thermal and chemical stability, remarkable mechanical strength and hardness, low prices, abundant reserves, and large-scale preparation. Therefore, silica-based ceramics still have good EMW absorption properties even at high temperature. The role of silica-based ceramics in EMW absorption mainly includes the following aspects. First, silica-based ceramics, as the base material, can contribute most of the dielectric loss or magnetic loss to the EMW absorber. Besides, the operability and remarkable mechanical properties of silica-based ceramics make it easy to recombine with other materials, thereby achieving good impedance matching. In addition, silica-based ceramics

based on structural design may have various EMW absorption mechanisms, such as interfacial polarization, dipole polarization, Debye relaxation loss, conduction loss, or multiple reflection. Naturally, the high thermal stability and oxidation resistance of silica-based ceramics make it play a major role in high-temperature EMW absorption.

3.1. Si-based oxides and alloys ceramics

3.1.1. SiO_2 composites

SiO_2 is one of the common components of EMW absorbing ceramics due to its unique physical and dielectric properties. From previous research, single-component absorbent often encounters several difficulties, including impedance mismatch, high density, and low thermal resistivity. These disadvantages can cause single-component absorbents to have low R_L and narrow effective bandwidth. The combination of SiO_2 can resolve some of these shortcomings. For example, Wang and co-workers had synthesized a structural ceramic silica/TiC by coating nickel-based superalloy on the mixture of silica/TiC/Al_2O_3 composites [118]. Experimental results showed that silica could significantly enhance the thermal resistivity of ceramic and allow it to work properly at temperatures up to 250 ℃. Both the real and imaginary parts of the complex permittivity increase with increasing temperature. Here, the permittivity of the composites increases with the increase of the TiC content, which can be ascribed to the improvement of the polarization ability and the increase of the electrical conductivity. More importantly, it creates better impedance matching by balancing the dielectric materials, which provides a reflection loss (R_L) of −55.2 dB at 11.8 GHz and an effective absorption bandwidth (EAB) of 3.2 GHz when the temperature reaches 150 ℃. Similarly, Ma et al. also used SiO_2 as a substrate to make SiO_2@TiO_2-C composite [119]. TiO_2 is an excellent candidate for EMW absorption due to its low density, excellent thermal stability, low cost, and environmental benignancy. However, to make TiO_2 achieve satisfactory EMW absorbing property, it needs to be hydrogenated first, which is an inconvenient process. Hence, reinforcing it with SiO_2 is an effective approach to overpass this barrier and increase its EMW absorption since SiO_2 provides impedance matching and interfacial polarization for ceramics. Notably, as the calcination temperature rises, the crystal lattice polarization gradually increases, resulting in the enhancement of the dielectric constant. In addition, the conduction loss also contributes to the dielectric capacity. It was found that the sample annealed at 650 ℃. has the best impedance matching and appropriate lattice polarization.

Apart from dielectric loss materials, magnetic loss materials also form functional ceramics together with SiO_2. Zhu and co-workers fabricated such composite using Ni and fly ash (FA), which is a silica-based solid waste in thermal power plants [120]. The SiO_2/Ni matrix (NiFA) was synthesized by the wet chemistry method, *in situ* carbothermal reductions, and calcination at various temperatures (Fig. 3a). The product displayed a surprisingly low density of 1.68~1.87 g cm^{-3}, which is much lower than conventional ferrite and magnetic cement, inferring its potential as an excellent EMW absorbing material. Furthermore, the sample demonstrated the outstanding compatibility of Ni and SiO_2. Firstly, the addition of Ni generates more interfacial polarization, and the abundant defects will produce dipole centers, leading to dipole polarization and enhancing the dielectric loss capability. Secondly, Ni/SiO_2 improves the impedance matching between magnetic loss and dielectric loss (Fig. 3c). Thirdly, the special porous structure of the matrix leads to additional paths for EMW, which provokes reflection

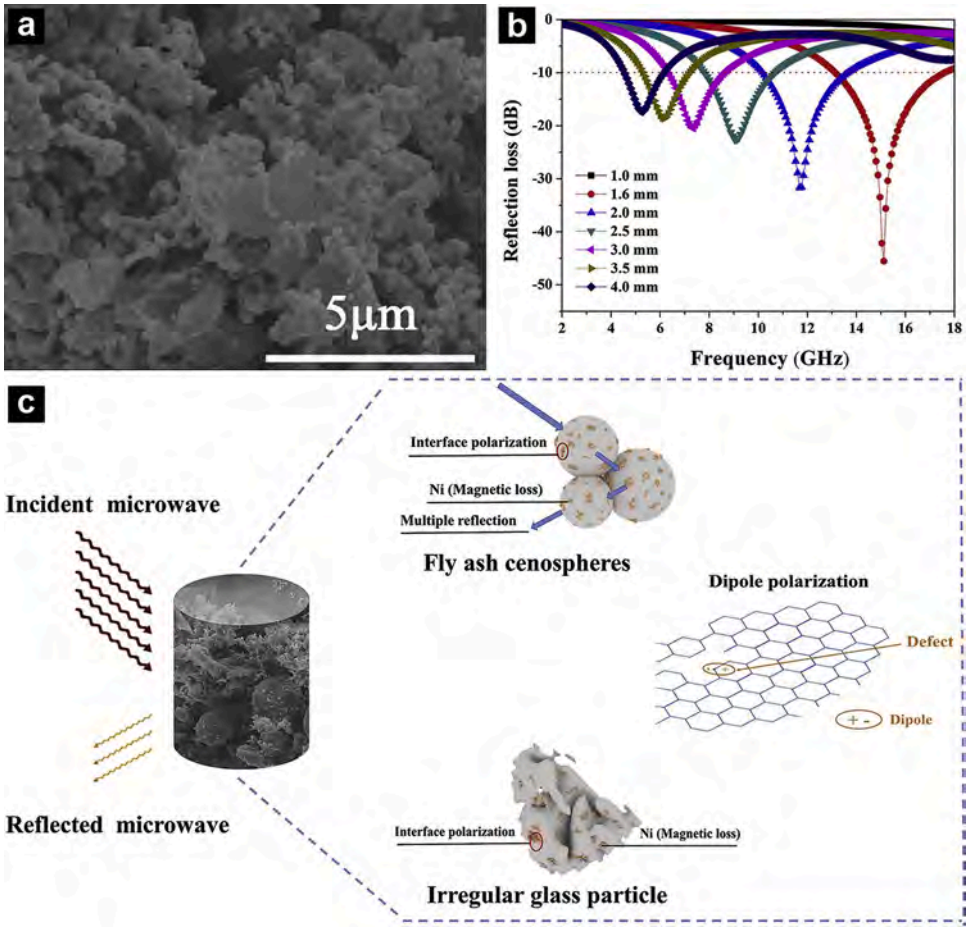

Fig. 3. (a) SEM image and (b) R_L value (at different thicknesses) of NiFA annealed at and 700 °C. (c) Scheme showing the possible EMW absorption mechanisms in NiFA composite. Reproduced with permission [120]. Copyright 2021, Elsevier.

and energy loss of EMW. These advantages help the resulting matrix to have a R_L of -45.7 dB at a thickness of 1.6 mm and an EAB of 4.6 GHz (Fig. 3b).

Overall, SiO_2 may not be a promising wave absorber. Nevertheless, it can ack as a skeleton to enhance the wave absorption ability of other dielectric or magnetic materials. By reinforcing the dielectric material with SiO_2, the composite matrix can have better permittivity at high temperatures due to the improvement of the polarization ability and the increase of electrical conductivity. More importantly, it can also increase impedance matching, which is an essential factor for reaching potential R_L. Likewise, combining SiO_2 with magnetic materials can also greatly improve impedance matching and polarization effect generated by the interface between the magnetic material and the matrix. It helps the composite matrix to maintain dielectric properties while keeping excellent wave absorption. It can be expected that if the designing process of magnetic/dielectric ceramics can be more concise and cheaper, it has the excellent potentiality of becoming a prevalent wave absorbing property.

Besides, reinforcing the SiO_2 matrix composite with carbon-based material can drastically improve its microwave absorbing ability. More importantly, by controlling the reaction cycle or time, the dielectric properties can be easily tuned. However, some considerations have to be taken into account when designing. If the carbon content exceeds some specific limit, it could potentially decrease the thermal resistivity of the SiO_2 composite and ruin the balance of impedance matching.

3.1.2. *SiO_2-carbon composites*

Carbon-based materials (*e.g.* CNTs, graphene, carbon fiber, porous carbon) have been widely investigated as EMW absorbents due to their excellent dielectric properties and low density [121,122]. However, high thermal conductivity and poor impedance matching hinder their application as high-performance EMW materials, especially in high-temperature environments [123]. Dong and co-workers addressed this problem by fabricating multifunctional SiO_2 ceramic (SiO_2/3A-l_2O_3·2SiO_2)-carbon nanowires (CNWs) [124]. The SiO_2 in the SiO_2-CNWs matrix provides superior thermal resistance to compensate for the high thermal conductivity of CNWs (Fig. 4a, b). Moreover, its low density and high porosity enable CNWs to grow efficiently by catalytic chemical vapor deposition (CCVD). The resulting SiO_2-CNWs ceramic showed conductive loss and polarization loss mechanisms, achieved a R_L of −31 dB, and had an EAB covering the whole X-band (8.2–12.4 GHz) (Fig. 4c, d). On the other hand, as the content of CNWs in the matrix increases, the EMW absorption capacity is significantly enhanced. However, too many CNWs will induce impedance matching imbalance, which is attributed to the higher permittivity of the material will bring strong surface reflection.

In addition, it is also essential to investigate the effect of temperature on SiO_2-carbon ceramic composites since they are commonly made for high-temperatures usage. For instance, the MWCNTs/SiO_2 composite was fabricated by filling the SiO_2-matrix composite with MWCNTs. The EMW absorbing properties were tested under different temperatures and frequencies [125]. As the temperature increases, the minimum R_L peak shifts to lower frequencies, and the value of R_L increases. Nevertheless, the magnitude of change largely depends on the content of MWCNTs and the thickness of the sample. The optimized results show excellent EMW absorbing properties with a R_L of −74.8 dB and an EAB of 4.2 GHz for MWCNTs/SiO_2 composites filled with 5 wt% MWCNTs. High microwave attenuation is related to the formation of a MWCNT micro-current network in the composites. The hopping and migrating electronic transport that occurs in it can be used to clarify the effect of MWCNT concentration and temperature on the conductivity, dielectric behavior, and microwave attenuation characteristics. SiC nanowires can also be used as fillers due to their low density and high oxidation resistance. For

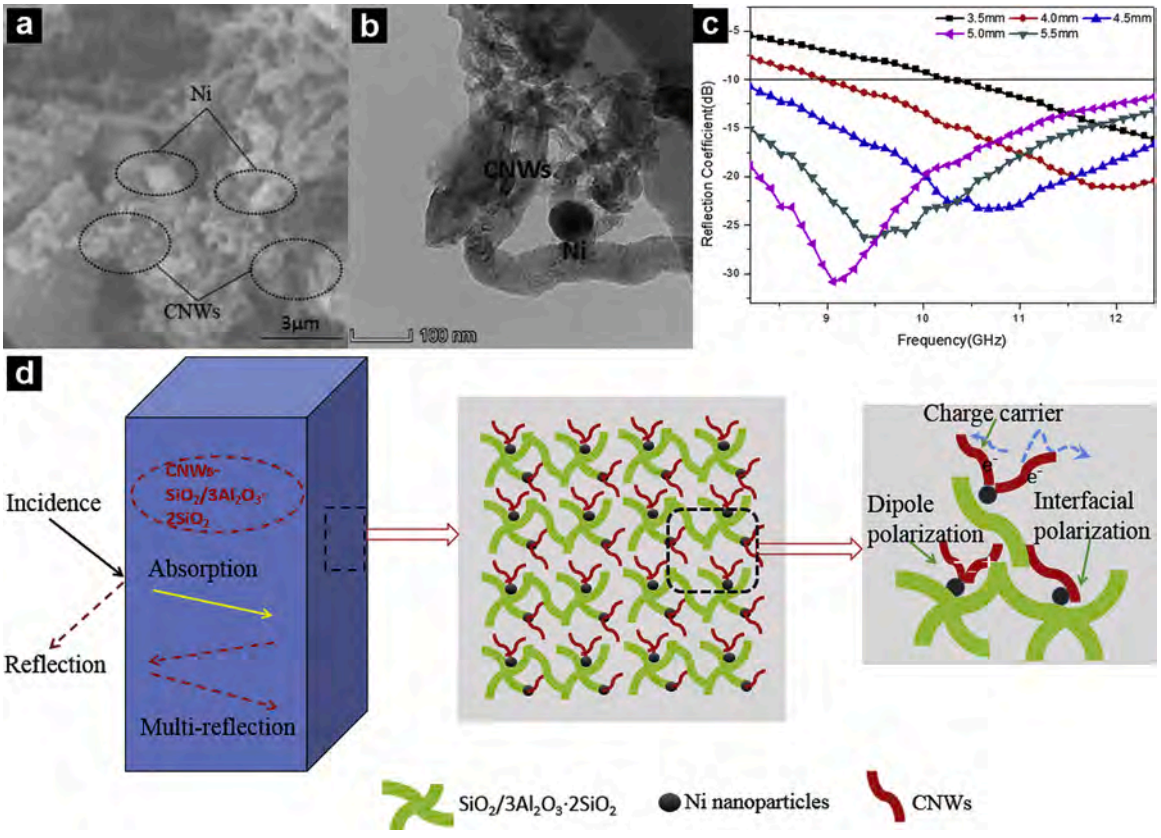

Fig. 4. (a) SEM image, (b) TEM image, (c) R_L value (at different thicknesses) of SiO_2-CNWs matrix. (d) Schematic illustration of EMW absorption in SiO_2-CNWs matrix. Reproduced with permission [124]. Copyright 2019, Elsevier.

example, Dong et al. synthesized $SiO_2/3Al_2O_3{\cdot}2SiO_2$ ceramics by the precursor infiltration pyrolysis process (PIP) [126]. The process continuously interleaves the conductive SiC nanowires to the base matrix, forming a porous 3D nanometer heterostructure. This structure has two main advantages. Due to the excellent conductivity, when the carrier moves within the microstructure or transports at the interface to form a micro-current, the conductivity loss will be enhanced. The porous structure will cause the EMW to scatter, deflect, and lose the energy within the ceramics due to interfacial polarization. Such characteristics make $SiO_2/3Al_2O_3{\cdot}2SiO_2$ ceramic a promising EMW absorbing material with a R_L of −30 dB at 10 GHz. Recently, the flower-like Co_3O_4@rGO/SiO_2 composites synthesized through a green fabrication route exhibit considerable EMW absorption properties (R_L = −52.6 dB, thickness = 1.78 mm) at a temperature of 80 ℃, which is attributed to the synergistic effect of magnetic loss, conduction loss, and multiple polarizations loss caused by the 3D hierarchical structures [127]. Specifically, porous Co_3O_4 flowers have multiple interfaces and pores, which bring magnetic loss and induce interface polarization and dipolar polarization. The residual defects and functional groups of rGO also induce strong dipolar polarization. The enhanced electron hopping is conducive to conduction losses at elevated temperature, which will enhance the EMW absorption performance.

3.1.3. Si-based multi-element oxides

Si-based multi-element oxides can achieve excellent microwave absorbing properties because they can effectively match with other wave absorbers. Even though carbon materials have extraordinary electric dissipation ability and low density, sometimes they fail to effectively absorb EMW due to their low permeability and impedance mismatching. This is when Si-based multi-element comes into play. For instance, Wei and co-workers used porous $Sc_2Si_2O_7$ as a matrix and reinforced it with CNTs using CVD technology (Fig. 5a) [128]. The scandium silicate matrix can create a 3D skeleton structure for CNTs to grow inside, thereby optimizing the effects of interfacial polarization and impedance matching, and the R_L reaches −33.5 dB at the thickness of 2.85 mm (Fig. 5b). The porous silica-oxide matrix generates an additional path for the EMW to travel, which sharply elevates the wave absorbing property. This extraordinary wave absorption ability is mainly due to the interfacial polarization formed between SiC and $Sc_2Si_2O_7$ and the increased impedance matching brought by SiC. Besides CVD, $Sc_2Si_2O_7$ ceramics can be composited with SiC through precursor infiltration and PIP to obtain good wave absorption due to the uniform distribution of C-rich SiC in the $Sc_2Si_2O_7$ matrix [129,130]. Meanwhile, defects, interfaces, and conductive networks in composites can improve the EMW absorption capacity.

In fact, Al-doped ZnO/$ZrSiO_4$ is also a promising wave absorbing material. Kong et al. synthesized such a matrix using the sol-gel process [131]. When the n-type semiconductor zinc oxide is combined with aluminum, it tends to generate more oxygen vacancies, which helps increase interfacial polarization and electric conductivity. On the other hand, zircon is a porous material with high thermal stability and insulation, which makes it a decent skeleton for zinc oxide. The combined matrix possesses suitable impedance matching and can be transformed into a flower-like structure with a complicated interface, and consumes EMW by interfacial polarization and deflection. The R_L of the Al-doped ZnO/$ZrSiO_4$ composite matrix is −32 dB, and the EAB is 3.6 GHz. Similarly, Liu et al. enhanced ZnO/$ZrSiO_4$ composites by adding Al_2O_3 powders [132]. When the content of Al_2O_3 is 3 wt%, the R_L of the composite can reach an −25.36 dB due to its high dielectric properties. However, the wave absorption worsens as more Al_2O_3 is added, which is

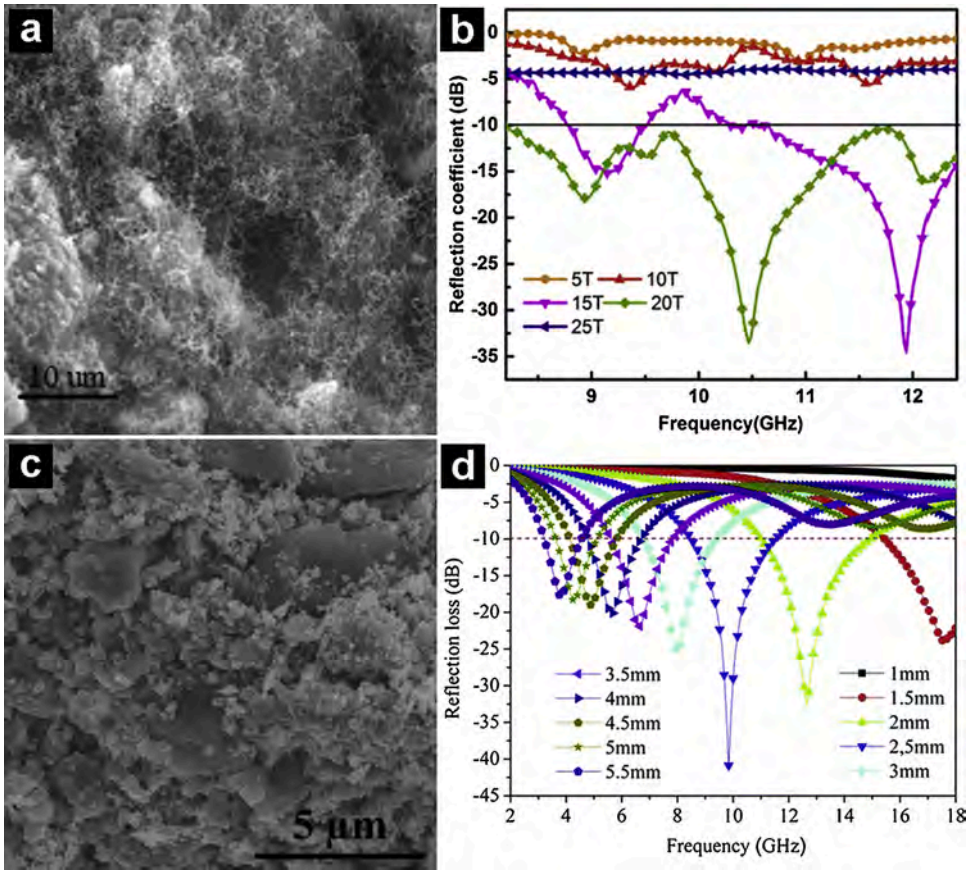

Fig. 5. (a) SEM image and (b) R_L value (thickness of 2.85 mm) of CNTs/$Sc_2Si_2O_7$ ceramics with various reaction times. Reproduced with permission [128]. Copyright 2019, Elsevier. (c) SEM image and (d) R_L value (at different thicknesses) of Fe_3O_4/Fe_2SiO_4 composite. Reproduced with permission [134]. Copyright 2020, Royal Society of Chemistry.

mainly due to impedance mismatching.

Apart from dielectric materials, Si-based multi-element oxides also match exceptionally well with magnetic absorbents. It advances the impedance matching between the dielectric and magnetic components in the matrix, which allows the resultant matrix to obtain considerable EMW absorption. For example, Li and co-workers fabricated rod-like ceramic Fe-Al_2O_3/$MgSiO_3$/$CaSiO_3$ [133]. Fe is commonly used as a magnetic adsorber due to its high abundance and low coercivity. Nevertheless, its high conductivity generates eddy currents, which increase EMW reflection and reduce efficiency. The oxide nanoflake-like shell containing Al_2O_3/$MgSiO_3$/$CaSiO_3$ attenuates this effect by suppressing the eddy currents and promoting EMW to enter the iron particles. As a result, the composite ceramic obtains both dielectric and magnetic properties that possess a R_L of −35 dB, and its EAB spans at least 2.56 GHz. Besides, Li et al. also reinforced iron with gangue, a coal mining industrial solid waste mainly composed of SiO_2, Al_2O_3, and FeS_2 [134]. The synthesis process of Fe_3O_4/Fe_2SiO_4 includes pelletizing gangue, *in situ* carbothermal reductions, and solid sintering (Fig. 5c). The resulting matrix had dielectric and magnetic loss mechanisms, and like the previous example, it has a facile synthesis process. Importantly, the interfacial polarization effect derived from the numerous interfaces between the loaded Fe_3O_4, carbon, and the matrix contributes to the high EMW absorption performance of the composite. The optimal ceramic possesses a R_L of -18.4 dB and an EAB of 4.2 GHz (Fig. 5d). In addition, other Si-based multi-element oxide materials such as Fe/FA [135], $CaMgSi_2O_6$ [136], and $Na_3Zr_2Si_2PO_{12}$ [137,138] have also been developed for EMW absorption.

In summary, Si-based multi-element oxides have excellent versatility and can work well with many different kinds of wave absorbers. Many combinations are shown unprecedented wave-absorbing ability. Thus, Si-based multi-element oxides have the potential to become promising wave absorbers and are worthy of further investigation.

3.1.4. Si-based metal alloy composites

Si-based metal alloy composites have attracted much attention as EMW absorbers due to their high thermal resistance and impedance matching with dielectric materials. However, such composites often face apparent flaws, including complex stacking and matching thickness, limiting their performance and practical applications. Among all Si-based metal alloys, FeSiAl alloy has stood out to be one of the best mainly due to its high permeability, low cost, good thermal stability, and flaky shape (prevents eddy current loss). For example, Qing et al. fabricated FeSiAl/flake graphite (FG)/Al_2O_3 ceramic using low-power plasma spraying [139,140]. The addition of FG allows the ceramic to have a second absorbent that effectively improves its absorption; moreover, it replaces a part of FeSiAl, which decreases the density of the ceramic and lowers the cost. The resulting matrix consumes EMW by polarization and magnetic loss. When the ceramic is exposed to an electric field, free electrons quickly accumulate in the interface between FeSiAl/Al_2O_3 and FG/Al_2O_3, thereby forming micro capacitors that lead to relaxation and interfacial polarization. Due to its various wave absorbing techniques, the matrix can attenuate an extensive range of EMW. The R_L values less than -7 dB can be obtained in the whole K_u band (12.4–18 GHz), with a thickness of only 0.8 mm. Instead of using FG and Al_2O_3, Zhou and co-workers used ZnO-filled resin to enhance the wave absorbing ability of FeSiAl [141]. Although ZnO is an excellent wave absorber due to its low density and dielectric properties, its excellent electrical conductivity often exceeds the threshold and destroys impedance matching. Zhou and co-workers improve this shortcoming by carefully adjusting the relative composition of FeSiAl and optimizing impedance matching. This allows the FeSiAl/ZnO-filled resin matrix to possess good magnetic dielectric loss. Also, the flaky shape of FeSiAl and the resin matrix provide a considerable specific area that generates multiple reflections and interfacial polarization, thereby making wave absorption better. The optimized matrix has a R_L of −40.5 dB at 10.4 GHz with an EAB spanning from 8.6–12.1 GHz.

Under the rapid development of aerospace engineering and civil engineering, the development of EMW absorbing ceramics has become a stringent task. Nevertheless, most ceramics whether failing to perform at high temperature or are easily oxidized. Guo and co-workers used a plasma-induced method to synthesize a core-shell FeSiAl/Al_2O_3/SiO_2 (FSA@GCLs) matrix to address this issue (Fig. 6a) [142]. This matrix has magnetic FeSiAl as the core and has two dielectricanti-oxidation layers on its outside surface (Fig. 6b, c). SiO_2 was used as the outermost layer because of its high thermal stability, anti-oxidation ability, and high microwave transmittance features. Al_2O_3 was used as a middle layer to reconcile the impedance matching and prevent damage from outside hazards, and FeSiAl was used as a magnetic EMW absorber as an inner core. This powerful combination gives the matrix a strong impedance matching. More importantly, the multilevel hierarchical shell structure provides abundant interfacial polarization and additional channels for EMW to scatter through. This highly thermally stable matrix was proven to perform under an extreme temperature of 1279 °C with an optimized R_L of −46.29 dB at 16.93 GHz and EAB of 7.33 GHz (Fig. 6d). In addition, Yang et al. also synthesized a heat-resistant Si-based metal alloy composite, C, N-codoped $MoSi_2$ [143], via solid-phase reaction. $MoSi_2$ has a low thermal expansion coefficient, a high melting point, elevated oxidation resistance, and excellent electrical conductivity. All of which suggests the potential of $MoSi_2$ being a strong EMW absorbent at high temperatures. The primary loss mechanism of this $MoSi_2$ matrix includes polarization loss and interfacial loss. When forming a matrix, SiO_2, Si, and $MoSi_2$ will generate a heterogeneous conductive network, just like myriad small capacitors. As EMW enters the matrix, the powerful multi-polarization resonance attenuates the EMW and produces a promising R_L.

Overall, Si-based metal alloy composites have great potential in aerospace and military applications due to their high thermal and oxidation resistance. Besides, they also possess numerous loss mechanisms and suitable impedance matching that optimize their wave absorbing ability. Despite the many advantages, there are still two significant improvements. First, the matrix can be thinner. Even though the shell-like matrix can sustain at high temperatures, it requires multiple layers to obtain such an ability. Second, the density can also be lower. As the composition of metal alloy increases, the thickness of the matrix increases rapidly. This can be a considerable problem and limit its use in many fields, especially in aerospace and military applications.

3.2. SiOC-based composite ceramics

Polymer-derived ceramics (PDCs) have been widely investigated as wave absorbers over the past years due to their suitable dielectric loss and high thermal and oxidation resistance. Among all PDCs, silicon oxycarbide (SiOC) stood out because of its unique anionic silica network, which helps maintain its chemical and mechanical durability. It can be easily synthesized using inexpensive low-temperature pyrolysis. These substantial advantages attract many researchers to study the EMW absorption properties of SiOC-based composite ceramics, as shown in Table 1.

3.2.1. SiOC and composites

Jia and co-workers synthesized an *in situ* partially surface-oxidized ultra-high-temperature ceramic (UHTC) SiOC/ZrB_2/ZrO_2 that could withstand up to 1000 °C (Fig. 7a) [146]. The introduction of ZrB_2 and ZrO_2 increases the impedance matching of SiOC and generates multiple interfaces between ZrB_2/SiOC and ZrO_2/SiOC. When EMW enters the ceramic, these interfaces generate dipole moments and provide substantial dielectric loss, consuming the energy of the EMW (Fig. 7b). Besides this mechanism, ZrB_2/SiOC also forms loops that induce current and excite electrons. As the loop size gradually increases, the permittivity increases and enhances the ability to absorb waves. This novel high-temperature EMW absorbing ceramic has a R_L of −29.3 dB, covering the whole Ka-band (Fig. 7c). Furthermore, Hou et al. also

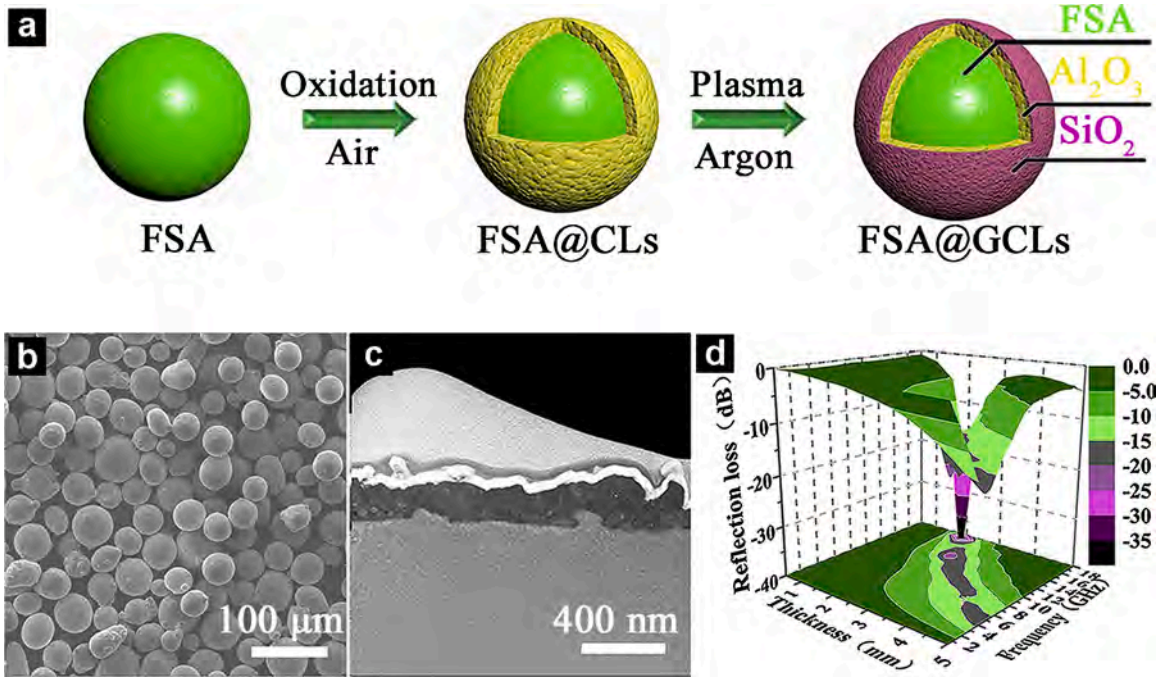

Fig. 6. (a) Scheme showing the synthetic process of FSA@GCLs. (b) SEM image of as-synthesized FSA. (c) SEM image of the cross-section of FSA@GCLs. (d) 3D R_L value of FSA@GCLs. Reproduced with permission [142]. Copyright 2020, Elsevier.

fabricated a highly thermostable (1000 °C) wave absorber SiCO/BN [147]. This ceramic has a core-shell structure with hexagonal BN as the core and SiOC as the shell. Different from common carbon wave absorbers that are unstable at high temperatures, SiOC/BN allows itself to retain the low transmission loss of hexagonal BN, while providing good thermal and oxidation resistance via the SiOC layer. As waves pass by, the microstructure also forms interfacial polarization and multiple scattering pathways, generating a dynamic electric dipole moment. It is suggested that high permittivity and permeability do not always lead to good reflection loss. Impedance matching (*Z*) usually must be between 0.8–1.2 to obtain optimized results. SiOC/BN also meets this requirement and proves SiOC and BN are an excellent match for each other. Therefore, the composite ceramic has a high R_L of -55.6 dB and EAB of 5 GHz.

Metallic wave absorbing materials like Fe can also match SiOC well. Fe ions tend to increase the carbothermal reaction at high temperatures and generate a large amount of SiC, which is beneficial for improving the dielectric properties. SiOC, on the other hand, provides Fe-based material a higher oxidation resistance at high temperatures. For example, Du and co-workers synthesized a Fe-doped SiC/SiOC nanocomposite via the solvothermal method [144]. Choosing an appropriate content for Fe ions allows SiC and turbostratic graphite to form in the amorphous matrix. When incident waves are applied to this amorphous matrix, the turbostratic graphite and SiC generate interfacial polarization, thereby improving the matrix's impedance matching and EMW absorption ability. The ceramic was found to have a R_L of −59.6 dB at 5.4 Hz and an EAB of 2 GHz. Similarly, Ma et al. also reported that Fe-doped SiOC ceramics showed good EMW absorption performance [145]. Among them, the formed Fe_3Si enhances the magnetic loss, and the SiC and turbostratic carbon produced by the PDCs process significantly increase the polarization and conduction losses. Moreover, magnetic particles Fe_3Si and dielectric particles SiO_2 improve impedance matching. Additionally, Hou and co-workers fabricated a novel Fe_3Si/SiOC ceramic via pyrolyzation [148]. Ceramics have an unusual ring shape, honeycomb structure. This structure has a high specific area that can accumulate positive and negative charges under alternating electromagnetic fields, which can further cause interfacial polarization and relaxation in the matrix. Moreover, Fe_3Si and SiOC also have good impedance matching, allowing more waves to be absorbed instead of reflected. Due to these advantages, Fe_3Si/SiOC is a promising EMW absorbing ceramic with a R_L of -41 dB and a broad EAB covering almost the whole S-band.

From the current research, we can see the potential of SiOC as an excellent wave absorber. It has tunable electromagnetic properties and high thermal and oxidation resistance. However, there are still some concerns to be addressed. Inappropriate iron content can lead to a drastic change in impedance matching. Hence, it requires extra consideration and care before synthesizing them in mass production. Other than that, SiOC-based ceramic seems to be a strong EMW absorbing candidate in space engineering.

3.2.2. *SiOC-carbon composites*

Given their dielectric properties, low-density features, and corrosive resistivity, nano-carbonaceous materials have become popular microwave absorbers. Nevertheless, the application for carbonaceous materials is often limited because of their low oxidation resistance. To retain the advantages of carbonaceous EMW absorbers and enhance their oxidation resistance, many researchers used PDC-SiOC to reinforce the composite ceramics. For instance, Zhao et al. fabricated a SiOC/carbon fibers (Cf) composite via a superficial precursor infiltration and PIP [150]. The matrix uses needled Cf as a skeleton and is reinforced with antioxidant SiOC particles. The optimal R_L value for this matrix was found to be −62.9 dB with an EAB of 14.7 GHz. Compared with other carbonaceous materials, Cf has a relatively higher thermal stability, bringing thermal stability up to 1000 °C. When the incident wave is applied to the matrix, it will be transformed into microcurrents by the 3D conductive network built by Cf, giving an intense rise in the dielectric loss. This Cf/SiOC composite can also be fabricated using boron-containing phenolic resin (BPR). The BPR method allows the matrix to possess higher temperature stability, which is mainly ascribed to the higher bond energy of B—O compared to CO— [154]. Furthermore, the heterogeneous interface of SiOC/Cfs structure forms multiple defects, interfacial and dipole polarization, which help to consume the EMW [157]. Hence, SiOC/Cfs composite has multiple wave-absorbing mechanisms, leading it to become an excellent wave absorbing material.

Table 1
Reported SiOC-based composite ceramics for EMW absorption.

Materials	Shapes	Methods	R_L and thickness	Ref.
Fe ions-SiOC	Sphere	Solvothermal method	−59.6 dB, 4.6 mm	[144]
Fe-doped SiOC	NPs	PDC	−20.5 dB, 2.8 mm	[145]
ZrB_2-SiOC	NPs	Thermal decomposition of polycarbosilane and PIP	−29.3 dB, 1.3 mm	[146]
SiCO@BN	Flake		−55.6 dB, 4.0 mm	[147]
Fe_3Si/C/SiOC	Honeycomb	Crosslinking and PIP	−41.0 dB, 3.5 mm	[148]
SiOC/C/melamine	Reticulation	PIP	−39.1 dB, 3.0 mm	[149]
SiOC + Cf	Fiber	Infiltration and PIP	−62.9 dB, 2.7 mm	[150]
SiOC/SiC_f/SiO_2	Fiber	Infiltration and PIP	−26.0 dB, 3.0 mm	[151]
Glucose + SiOC	Nanowire/NPs	Solvothermal and pyrolyzation	−27.6 dB, 1.6 mm	[152]
Al_2O_3/CNTs/SiC/SiOC	Nanowire	3D-printing	−56.8 dB, 2.8 mm	[153]
SiOC + Cf	Needle	Infiltration	−24.3 dB, 1.1 mm	[154]
CNTs + SiOC	Nanotube	PIP	−60.4 dB, 3.5 mm	[155]
SiOC + Cf	Nanorod	PIP	−47.5 dB, 5.1 mm	[156]
SiOC + CNFs	Porous backbone	PIP	−47.9 dB, 2.3 mm	[157]
SiOC/$FeCl_3$/SiC/CNTs	Needle-like	PIP	−58.4 dB, 3.0 mm	[158]
SiOC/SiC/C	Complex structure	PDC	−23.4 dB, 1.6 mm	[159]
SiOC/SiCnws/CFs	Nanowire	Infiltration and PIP	−48.2 dB, 3.6 mm	[160]
SiOC/$FeCl_3$/CNTs	Nanotube/NPs	Infiltration and PIP	−35.5 dB, 2.9 mm	[161]

Note: CFs represent carbon fiber felts, Cf represents carbon fibers, CNFs represent carbon nanofibers, NPs represent nanoparticles, PIP represents the pyrolysis process, PDC represents the polymer-derived ceramics.

Mei and co-workers also used PIP to synthesize their compounds with Al_2O_3, CNTs, SiC nanowires, SiOC via 3D printing [153]. Even though Al_2O_3 itself does not possess good dielectric properties, it could be used as a substrate to grow SiC nanowires. SiC, contrarily, is an excellent dielectric material with good wave absorbing ability. Combining CNTs and SiC nanowires generates a conductive 3D network and provides a dielectric loss and conductive loss mechanism for the composite. However, the impedance matching has to be controlled with care since CNTs acquire high dielectric loss properties. As the content of CNTs exceeds 5 wt%, the impedance matching of the matrix is ruined and causes EMW to deflect. With proper CNTs content, Al_2O_3/CNTs/-SiC/SiOC composite can achieve a minimum R_L of -56.84 dB at 12.2 with an EAB ranging from 8.2–12.4 GHz, covering the whole X-band. It is also noteworthy that agglomeration during PDC preparation processes can enormously hinder ceramics wave absorption. Fortunately, this issue can be solved by introducing catalytic pyrolysis with $FeCl_3$/polysiloxane as a precursor [158,161]. The catalytic pyrolysis prevents aggregation and enhances the formation of nanostructures, giving the resultant matrix outstanding wave absorbing and dielectric abilities.

Besides, glucose has received much attention ascribed to its high electrical conductivity and dielectric property. Du and co-workers made a glucose-derived carbon-rich silicon oxycarbide (glucose-SiOC) via solvothermal process and pyrolyzation (Fig. 8a) [152]. This composite matrix has a heterostructure with SiOC as the base, decorated by glucose-derived carbon and SiC particles (Fig. 8b). The introduction of glucose brings two main advantages. First, it supplies SiOC ceramics with greater interfacial polarization and conductive loss. Second, it balances the impedance matching of the SiOC ceramic, which allows a minor fraction of waves to be deflected. This glucose-SiOC ceramic has an optimal R_L of -27.6 dB at a thickness of 1.5 mm and an EAB of 3.5 GHz (Fig. 8c). Despite the fact that glucose-SiOC ceramic has relatively weaker EMW absorbing ability compared to other typical PDC absorption composite (SiBCN, Co, or Fe-containing SiC/C systems), it shows significant enhancement compared to pure SiOC, plus the fact that it has a great potential to further improve by incorporating metal elements such as Co, Fe, and Ni. Also, there are some novel ways to make PDC-SiOC based ceramics. For instance, Chen et al. manufactured a C/SiC/SiOC porous network through the pyrolysis of dimethyl silicone oil, silane coupling agent, and melamine foam [149]. The resultant matrix forms a reticulate porous structure. As the incident wave enters the ceramic, the porous structures act like numerous micro capacitors under an external electric field and deplete wave energies. SiC and nano carbons serve as electrically lossy phases dispersed in the matrix, creating abundant interfacial and dipole polarization, which helps to dissipate EMW.

To summarize, carbonaceous materials are very compatible with PDC-SiOC ceramics ascribed to their low mass, strong absorbing stability, and thin thickness. Although not mentioned in the previous paragraphs, the nano carbons in all these examples form 3D nanostructures. Hence, they will generate complex scattering paths for EMW to pass by, which is also an essential factor in EMW conductive loss. Some significant advantages of this type of carbonaceous composite are that they have acquired many kinds of EMW absorbing techniques, and can be easily synthesized and tuned to meet the desired functions.

3.3. SiC-based composite ceramics

SiC is a wide bandgap semiconductor with outstanding mechanical and dielectric properties. It can tolerate high temperatures and form numerous structures while maintaining its dielectric properties at the same time. For this reason, plenty of researchers have been studying ways to improve the EMW absorbing properties of SiC-based composite ceramics, such as SiC and composite and SiC-carbon composite, as shown in Table S1 (details in Supplementary Information) [162–218].

3.3.1. SiC and composites

A specific enhancement of SiC is to build a core-shell structure with various magnetic and dielectric components. For example, Gu et al. fabricated a novel core-shell structured Fe_3Si@C/SiC/Fe_3O_4/SiO_2 nanoparticles with Fe_3Si as the core and C/SiC/Fe_3O_4/SiO_2 as the shell [178]. The most crucial characteristic of this magnetic core-shell structure is that it possesses magnetic loss and dielectric loss mechanisms. When an incident wave is applied, the wave is first destructed by the outer surface of the dielectric made of SiC. This layer generates surface polarization and forms interfacial polarization in the phase interface holes. As the wave continues to penetrate the center core, it is then further attenuated by the inner Fe_3Si (a typical nanoparticle with excellent ferromagnetic properties). This dual wave absorbing mechanism ensures the efficiency of absorbing. This matrix reaches a R_L of −44.7 dB and has an EAB from 2.5 to 12.0 GHz, covering the whole X and C bands.

Traditional magnetic absorbers tend to lose their magnetic loss property at temperatures higher than their Curie temperature, and dielectric absorbers have poor oxidation resistance at high temperatures. Therefore, absorbers that can function at high temperatures are desirable. Thermal stability is also a typical trait of SiC. Jian and co-workers synthesized a heterogeneous $ZrN_{0.4}B_{0.6}$/SiC nanohybrid via CCVD and chemical vapor infiltration (CVI) process [169]. Even though ZrB_2, the starting material, is not a sound-absorber itself, by reinforcing it with N atoms and SiC, it becomes an excellent absorber with high thermal resistance. Moreover, the interface between $ZrN_{0.4}B_{0.6}$ and SiC

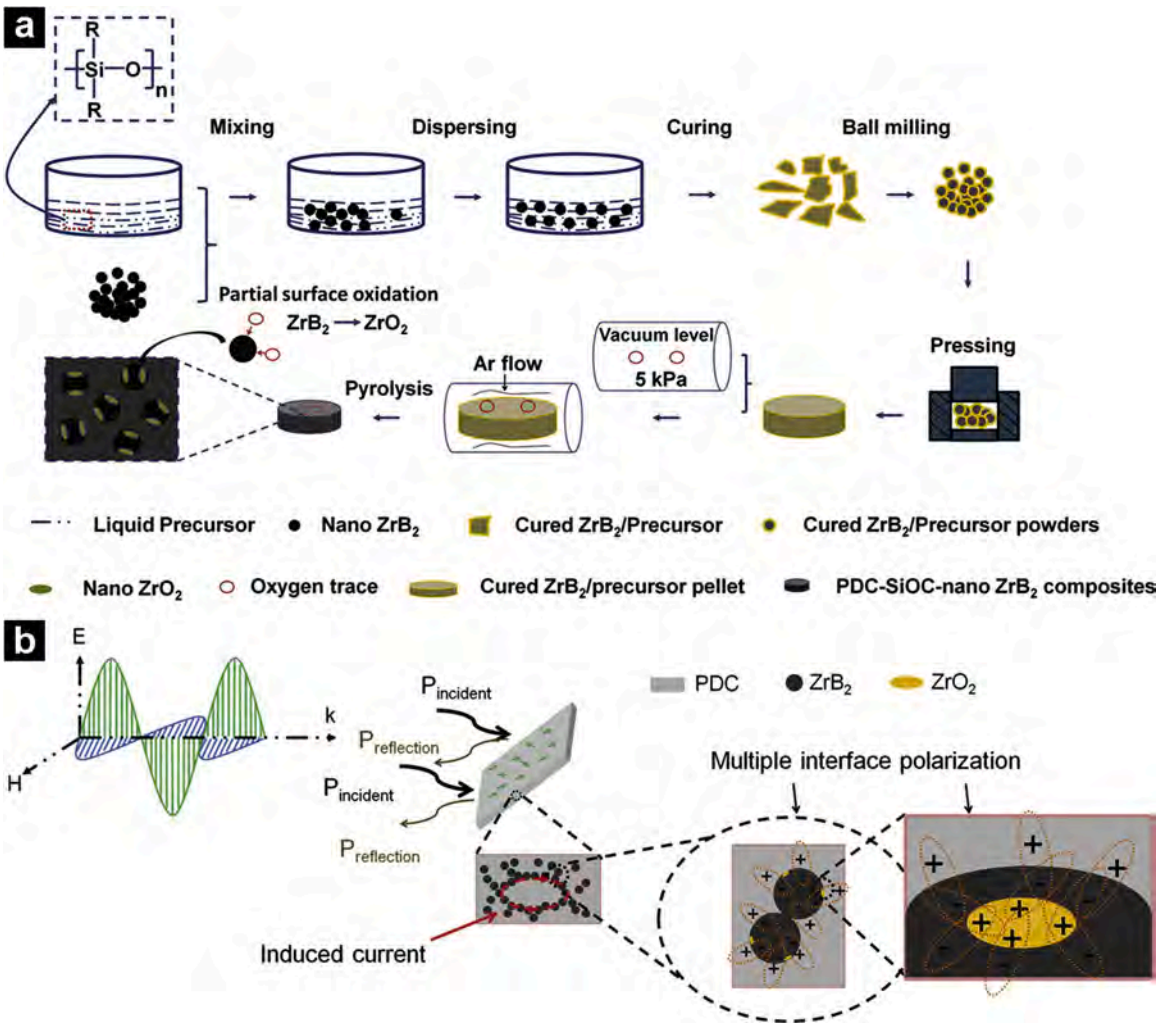

Fig. 7. Scheme showing the fabrication process (a) and EMW absorption mechanism (b) of the SiOC/ZrB_2/ZrO_2 composites. Reproduced with permission [146]. Copyright 2019, American Chemical Society.

can form numerous defects and interfaces, which is very beneficial for Debye relaxation, Maxwell-Wagner relaxation, polarization, and multiple scattering. This matrix was tested at high temperatures up to 600 °C and sustained gratifying results in wave absorption and antioxidative features. The R_L is −50.8 dB at 7.7 GHz at a thickness of 3.05 mm. Besides using $ZrN_{0.4}B_{0.6}$, Huo et al. produced a high temperature and oxidation resistance composite using the SiC/ZrC/SiZrOC hybrid nanofibers [170]. This matrix was fabricated via electrospinning and high-temperature pyrolysis processes. ZrC was chosen because it has a relatively low price compared to other materials like HfC and TaC. More importantly, its high melting point, high stiffness, and satisfactory electrical conductivity make it a good match with SiC nanofibers. Combining the two materials can improve high-temperature oxidation resistance and generate plentiful interfacial polarization, which is beneficial to high-temperature EMW absorbing properties. As the ZrC content increases from 0 to 10 %, the Debye relaxation loss and conductivity loss of the resulting matrix continue to grow, maximizing the absorbing ability. The composite was found to function at 600 °C, with an optimal R_L of −40.38 dB at 14.1 GHz.

Although the PIP-derived SiC composite can provide excellent thermal resistance, it shows poor wave absorbing property due to the strong conductive network formed by free carbon. Increasing heat treatment is a facile way to remove excess carbon, but the adverse effects are apparent as well. Increased heat treatment will produce oxidation channeling at high temperatures and cause fiber degradation. Another alternative of removing carbon is to dope active fillers such as Ti, Cr, Mo, Al, and $CrSi_2$ into the precursor. Ti powders, for example, can actively react with carbonaceous species, forming TiC and destroying carbon networks [173], allowing us to effectively adjust the impedance matching.

3D printing is a novel way of preparing ceramics. It provides numerous advantages that cannot be obtained with conventional preparing methods, including straightforward modeling, homogenous dispersion, and mass production. For example, Xiao et al. fabricated a SiC nanowire/acrylic resin via 3D stereolithography printing technology [196]. Since the 3D stereolithography printing uses liquefied Methacrylic acid esters as raw materials, SiC nanowires can be uniformly dispersed in the solution. In addition, using liquefied raw materials also opens the door for printing complex structures. The final composite was found to exhibit excellent precision in printing and great wave absorbing properties. Furthermore, 3D printing technology and CVI have been used together to synthesize a 45 ° V-type honeycomb Al_2O_3/SiC whisker composite with many channels and walls (Fig. 9a–c). Such a matrix can achieve a remarkable R_L of −63.65 dB at a thickness of 3.5 mm owing to multiple wave reflections within the honeycomb structure (Fig. 9d–f) [183]. When EMW is incident on the surface of the Al_2O_3/SiC whisker, more waves can enter the channels of the oblique honeycomb structure, and other waves are reflected into the air. Furthermore, the incident wave passes through the SiCw surface, resulting in high dielectric loss and energy drop. In addition, the interface between SiC and Al_2O_3 will

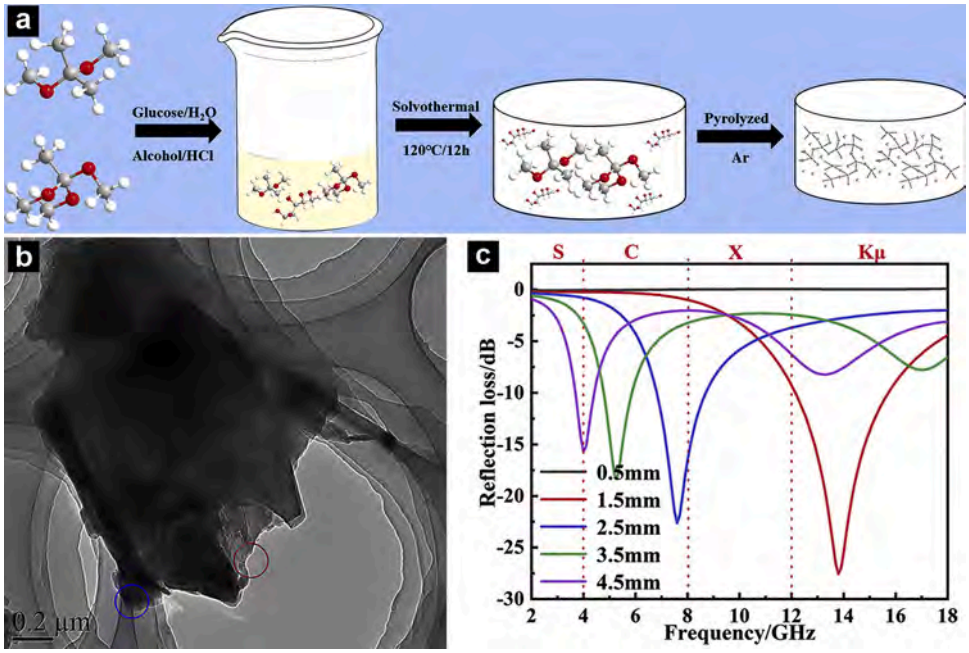

Fig. 8. (a) Illustration of synthetic process of glucose-derived carbon-SiOC ceramics. Corresponding TEM image and R_L value at different thicknesses. Reproduced with permission [152]. Copyright 2019, John Wiley & Sons, Inc.

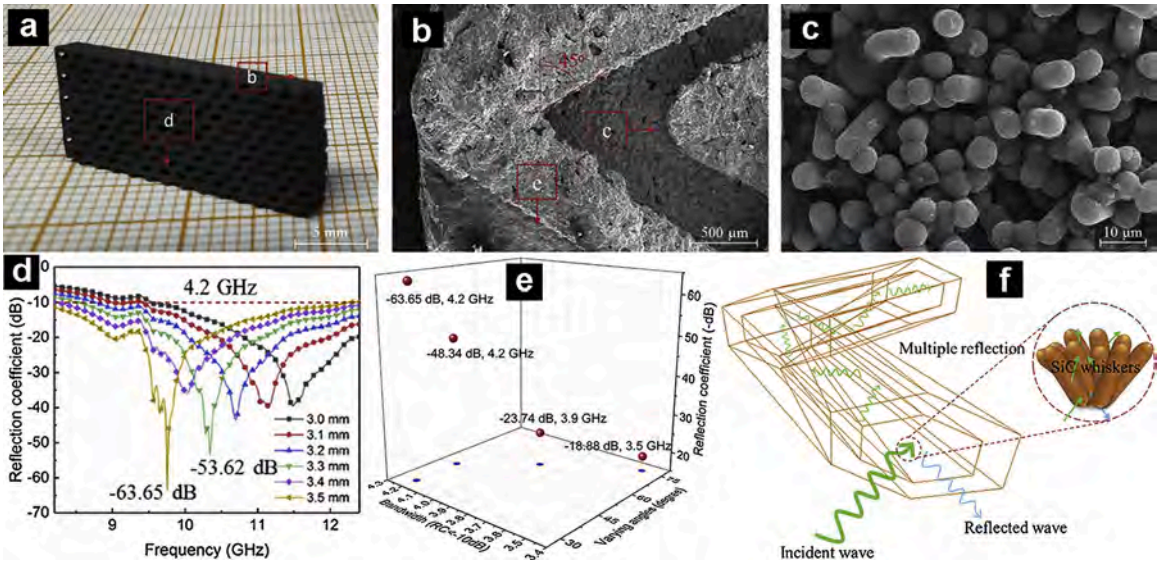

Fig. 9. (a) Photograph of the specimen. (b,c) SEM images, (d) R_L value (at different thicknesses), (e) R_L value with varying angles, and (f) EMW absorption mechanisms for the 3D printed Al_2O_3/SiC whiskers composites. Reproduced with permission [183]. Copyright 2019, Elsevier.

cause interface polarization, which is also conducive to EMW absorption. Even though the honeycomb structure can be difficult to fabricate using the conventional method, 3D printing technology makes it easier to modify and build each part.

To conclude, SiC is a promising additive phase for wave absorbers due to its high thermal resistance, wear resistance, high strength, designable microstructure, and high surface area. It can be synthesized with ferrite components and generate an outstanding composite that acquires both dielectric loss and magnetic loss. Furthermore, it can also be synthesized with other dielectric components to create high-temperature resistance wave absorbers. Thus, SiC composites are potent candidates for novel wave-absorbing materials.

3.3.2. SiC-carbon composites

Although SiC has many advantages as an absorber, pure SiC usually results in low EMW absorption. Thus, SiC usually requires a second phase absorber to maximize its wave absorption. Researchers have found carbon-based materials closely match SiC ascribed to their low densities, high electric conductivity, and significant dielectric loss. The most common type of such SiC-carbon composites is SiC/C nanofibers. For example, Wang et al. developed a one-dimensional C/SiC hybrid nanocomposite via electrospinning of polycarbosilane (PCS) and polyvinylpyrrolidone (PVP) followed by pyrolysis and annealing treatment [201]. This C/SiC hybrid nanocomposite composes mainly SiC and C nanofibers, which has the advantage of maximizing active surface to volume ratio and maximizing conductive loss. Furthermore, the accumulation of charges on the heterojunction interfaces will induce

electrical dipole moments between SiC and C nanofibers, making them act like micro capacitors that generate interfacial polarization and dipole polarization. Under these circumstances, the wave absorbing ability of SiC/C nanocomposite increases drastically compared to SiC or C fibers alone. One concern with SiC/C nanofibers is that carbon has high electrical conductivity, which usually leads to impedance mismatches. Wan and co-workers suggested that the introduction of Al_2O_3 has a significant effect on balanced impedance matching [212]. With the increase of carbon black content, the real and imaginary parts of the complex permittivity increase in the X-band. However, there is a noticeable enhancement in absorption property of SiC/Al_2O_3/C with the assistance of 5~15 wt% Al_2O_3.

Besides, reduced graphene oxide (rGO) foams have also been widely studied as wave absorbers because of their internal conductive network, low density, excellent mechanical resistance, and dielectric properties. Nevertheless, rGO has terrible oxidation resistance, which limits its application in many fields. One way to resolve this issue is to incorporate SiC nanowires into the rGO foams. By doing this, rGO could keep its excellent wave absorbing properties while having great thermal stability from SiC at the same time [208]. For instance, Han and co-workers fabricated a 3D rGO/SiC nanowire foam composite via freeze-drying and carbothermal reduction processes (Fig. 10a–c) [206,209]. The resultant matrix has two major wave absorbing mechanisms. First, the 3D hierarchy of the matrix creates additional paths for waves to travel and causes further conduction loss within the matrix. Second, the high-density stacking faults between rGO and SiC nanowires can produce multiple interfacial polarization that dissipates waves (Fig. 10d). These two powerful mechanisms enable the rGO/SiC nanowire foam composite to obtain gratifying wave absorbing performance while maintaining high thermal stability above 630 °C. The matrix achieves a R_L of -27 dB and has an EAB covering the whole X-band (Fig. 10e).

Furthermore, SiC/C anti-oxidant composites can also bind with magnetic absorbers like ferrite to improve their wave absorbing properties. For example, Hou et al. synthesized a novel high-temperature anti-oxidative SiC/Fe_3Si/CNTs composite from Fe-containing polydiacetylene (PSA) [210]. This composite was proven to have excellent wave absorbing performance due to several reasons. First, the interfaces between spherical Fe_3Si, SiC, and CNTs accumulate a large amount of positive and negative charges when applied to an electric field, causing multiple interfacial polarizations that help dissipate waves. Second, with the introduction of Fe_3Si, the composite has appropriate impedance matching that can absorb the wave to the maximum. Lastly, having both magnetic and dielectric loss mechanisms guarantees the matrix to have lower reflection loss and broader bandwidth than pure components. The antioxidant characteristic was tested at 800 °C hot air, and the results showed that only 4.9 % of the mass was lost in such a harsh environment. This absorber exhibits excellent antioxidant ability and maintains a minimal R_L of -40 dB at 10.36 GHz with the EAB ranges from 10.4 to 15.2 GHz.

To conclude, although the addition of carbonaceous components will reduce the thermal stability of SiC composites, SiC-Carbon composite can still be viewed as promising wave absorbers at mild temperatures. Regarding thermal stability, studies have shown that the thermal resistivity of SiC-carbon composites can be improved by adding a third component or adjusting the content of carbon material. Hence, SiC-carbon composites are worthy of further study.

3.4. Si_3N_4-based composite ceramics

With the rapid development of military and space engineering, high-temperature radar absorbing materials (HTRAMs) are highly demanded due to their high oxidation resistance, mechanical strength, and low density. For a ceramic to have high thermal resistance, the ceramic has to possess low dielectric loss. Therefore, materials like SiO_2, hexagonal BN, and Si_3N_4 turn out to be promising candidates for high-temperature resistive materials. Among them, Si_3N_4 is a more appropriate choice in military use because it has superior toughness compared to SiO_2 and has better mechanical performance compared to BN. At this point, Si_3N_4-based composite ceramics deliver an existing EMW absorption performance, as shown in Table S2 (details in Supplementary Information) [219–247].

3.4.1. Si_3N_4-carbon composites

Si_3N_4 matches well with carbonaceous materials. Research has found that a proper content of carbonaceous materials can enormously increase the dielectric constant and reduce the electromagnetic reflectivity [219,223]. For instance, Saleem et al. synthesized a fluoride-doped MWCNT/Si_3N_4 composite via hot press sintering [224]. Even though

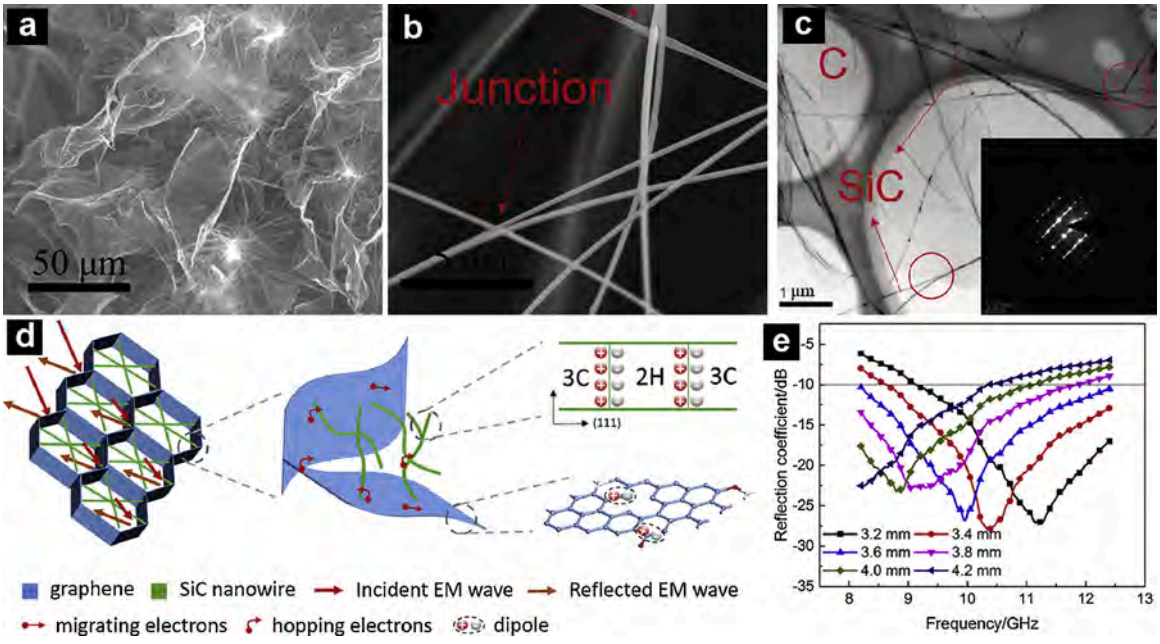

Fig. 10. (a,b) SEM image, (c) TEM image, (d) schematic for the EMW absorption mechanism, and (e) R_L value (at different thicknesses) of rGO/SiC foam composite. Reproduced with permission [206]. Copyright 2017, American Chemical Society.

pure Si_3N_4 does not show outstanding EMW absorbing performance, as the content of MWCNT increased, a substantial improvement in wave absorption was established. This is mainly due to the multiple interfacial interactions formed between Si_3N_4 and MWCNT, which sharply increases the real part of the permittivity and wave dissipation process. Hence, this investigation shows that adding carbonaceous materials enhances the EMW absorbing performance of Si_3N_4/carbon-based matrices. Luo et al. also built a multilayer Si_3N_4/Cf composite and tested it for its high-temperature dielectric behavior [220]. Such composite displays excellent permittivity and loss tangent within the range of 25–800 °C, while the permittivity shows a strong dependence on the wave frequency. The excellent temperature stability is mainly due to the unique graphic planes of carbon, which helps increase electric polarization and relaxation of electron migration.

Another way to reinforce Si_3N_4 is by adding rGO. rGO is also a member of carbonaceous materials that exhibit a high surface-to-volume ratio, excellent carrier mobility, and abundant defects. These traits make rGO a powerful candidate for wave absorbents. For instance, Hou et al. developed a 3D sandwich-like Si_3N_4/rGO composite using a freeze-drying approach and CVI process [222]. The 3D crosslinking structure endows the ceramic to have high porosity with abundant interfacial polarizations formed inside. Unlike other carbonaceous materials (e.g., carbon nanowire, CNTs) that mainly consume waves through conductive loss, 32 % of the total dielectric loss Si_3N_4/rGO comes from polarization loss. This characteristic ensures that ceramic retains stable impedance matching as the temperature continues to increase, whereas other carbon materials lose the balance between conductivity and polarization relaxation. This unique phenomenon enables the ceramic to obtain outstanding temperature-independent performance in EMW absorption. Si_3N_4/rGO can function at a temperature ranging from 323 to 873 K, with an EAB covering the whole X-band.

Graphene has a perfect planar structure, which gives it a higher conductivity and more significant dielectric loss due to the hopping conduction behavior and capacitive character [221]. However, high conductivity often causes a better chance of impedance mismatching, which lets the ceramic reflect wave rather than absorb it. Ye and co-workers introduced edge-like structures into CVD graphene to address the problem (Fig. 11a) [247], enhancing the conductive loss and increasing the number of intrinsic defects. By doing this, the matrix obtained lower electrical conductivity and better impedance matching. Different from 1D carbonaceous materials like CNTs, the edge-rich graphene/Si_3N_4 can wrap around the Si_3N_4 whiskers (Fig. 11b),

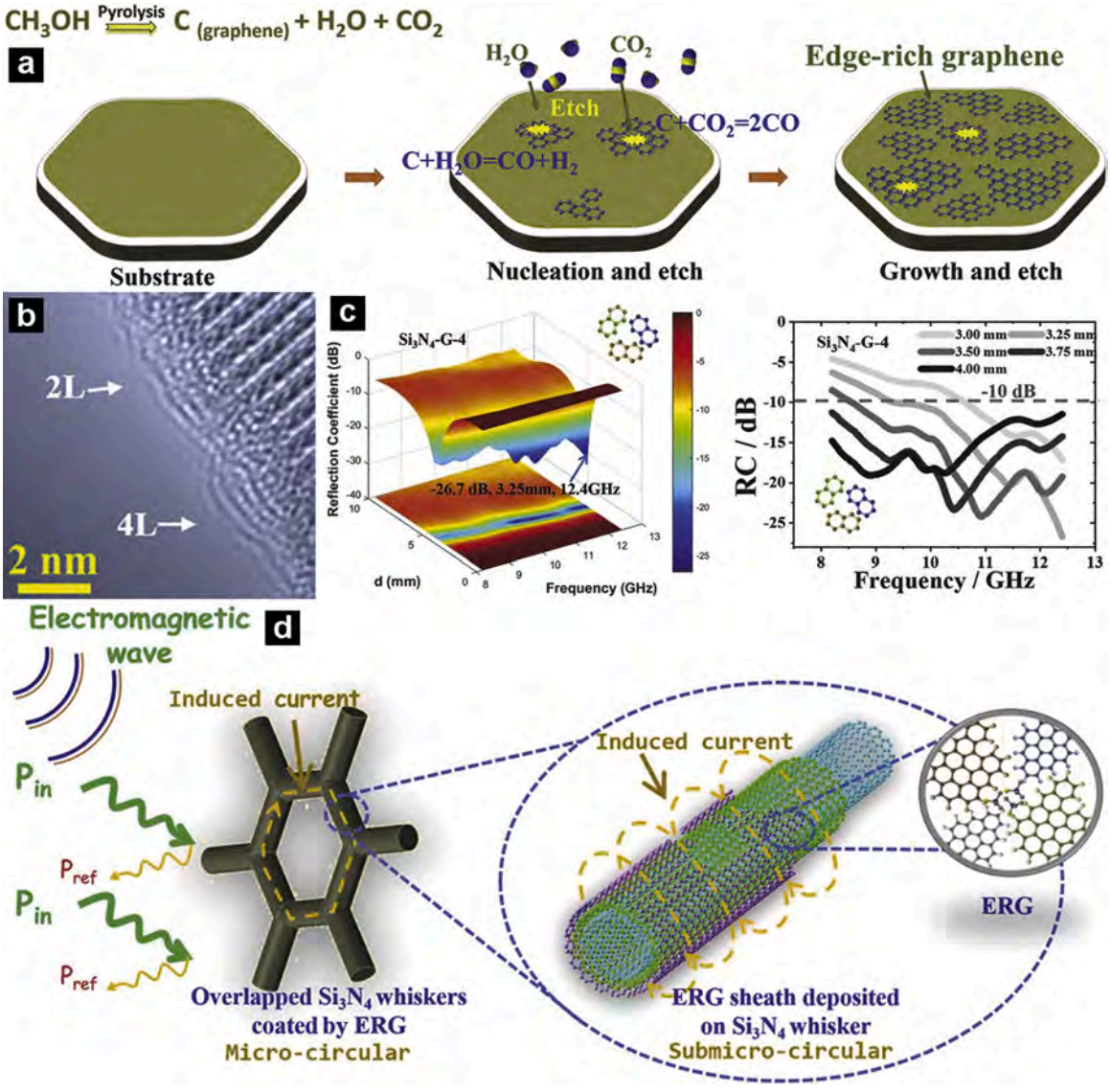

Fig. 11. (a) Scheme showing the synthetic process, (b) TEM image, (c) 3D R_L value and reflection coefficient (at different thickness), and (d) scheme showing the EMW absorption mechanisms of ERG/Si_3N_4 hybrids. Reproduced with permission [247]. Copyright 2018, John Wiley & Sons, Inc.

forming hierarchical structures that act like enormous resistance-inductance-capacitance coupled circuits (Fig. 11d). Such construction has been proven to be very effective in converting long-range-induced currents to thermal energy. Due to the huge resistance-inductance-capacitance coupling circuit and the time-varying electromagnetic field-induced current on the edge-rich graphene (ERG)/Si_3N_4, the hierarchical circular structure strongly responds to the broadband incident microwaves. This long-distance-induced current decays rapidly in the resistive network and is converted into heat energy, resulting in the rapid attenuation of a large number of incident EMW. The effective EAB of this ERG/Si_3N_4 ceramic was found to be 4.2 GHz, covering the whole X-band (Fig. 11c).

In conclusion, Si_3N_4/carbon composites seem to be promising wave absorbers, especially at relatively high temperatures. They generally have a higher minimum reflection loss than other Si-based composites. There is also far less research on them than SiC/carbon composites and SiO_2/carbon composites. As a result, Si_3N_4/carbon composites may be an excellent novel wave absorber but require more future research to assert.

3.4.2. *Si_3N_4-SiC composites*

As mentioned in the previous chapters, Si_3N_4 and SiC are excellent components for thermal resistive absorbers due to their anti-oxidation properties, high mechanical strength, and chemical stability. Moreover, since they can be fabricated into structures like nanowires and nanotubes, they have a higher active surface-to-volume ratio, which strongly enhances the dielectric loss. Because of these advantages, Si_3N_4/SiC composites are widely investigated in recent years. Wang et al., for example, synthesized graphite/SiC/Si_3N_4 composite via electrospinning technology. In this matrix, graphite acts as the main conductive phase to dissipate wave energy [236]. SiC and Si_3N_4, on the other hand, are served as the semiconductor phase and EMW transparent phase, respectively. Since SiC has its real permittivity higher than imaginary permittivity, while Si_3N_4 has its real permittivity lower than imaginary permittivity, the composite using only SiC, or Si_3N_4, often leads to impedance mismatching. However, with the proper content of graphite/SiC/Si_3N_4, the composite matrix shows excellent impedance matching while keeping outstanding chemical and physical properties. Also, the graphite/SiC/Si_3N_4 composite heterostructure also plays an essential role in wave absorption. Electrons were found to jump between nanofibers when applied to an alternating electric field, accumulating positive and negative charges on the interface. This phenomenon can then lead to a large amount of interfacial polarization and give rise to dielectric loss. The composite matrix exhibits a strong R_L of -57.8 dB and a wide EAB of 6.4 GHz.

Although Si-based ceramics have lots of advantages, including good dielectric loss, low densities, high strength, etc., they are brittle and have low fracture toughness, which limits their use in many fields. One way to solve this problem is to reinforce and toughen them using continuous fibers. SiCf/Si_3N_4 composite has been proven to be one of the best candidates due to its unique porous structure. CVI-derived SiCf/Si_3N_4 was reported to form inter-bundle pores across the whole matrix (Fig. 12a, b) [235]. Such pores improve the fracture toughness through crack deflection and crack bridging, in which different fiber bundles act as a single toughening unit and increase the crack propagation path. With this powerful mechanism, SiCf/Si_3N_4 displays better flexural strength and fracture toughness compared to conventional wave absorbing ceramics (Fig. 12c, d).

Recently, freeze casting has gained much attention, mainly attributed to its environmental friendliness and the flexibility to control the porous structure of ceramics [237,238]. For instance, Hong et al. fabricated a porous PDC-SiC/Si_3N_4 via freeze casting method along with different content of polycarbosilane (PCS) [237]. As the content of PCS increases, more Si_3N_4 nanowires begin to form. Moreover, the compressive strength and the porous structure of Si_3N_4 also experienced enhancement noticeably as the content of PCS increases. This transformation in the microstructure gives rise to the formation of polarization centers, which drastically improves R_L from -20.2 dB to -56.2 dB. In addition, the abundant interfaces between Si_3N_4, *in situ* formed PDC-SiC nanograins, nano-sized carbon and Si_3N_4 nanowires enhance electronic dipolar polarization and interface scattering.

Another benefit of SiC/Si_3N_4 composite is their reliable high-temperature wave absorbing performance. Since SiC and Si_3N_4 have a smaller thermal expansion coefficient than other materials, their size of the period patterns is relatively more stable at a higher temperature. Zhou et al. utilized this advantage and developed a meta-structured SiCf/Si_3N_4 composite via the CVI technique [241]. The most exciting aspect of this matrix is its grooved crossing structure, which provides two benefits for this matrix. First, the grooved system has a more stable effective impedance (Z_{eff}) at various temperatures compared to the flat

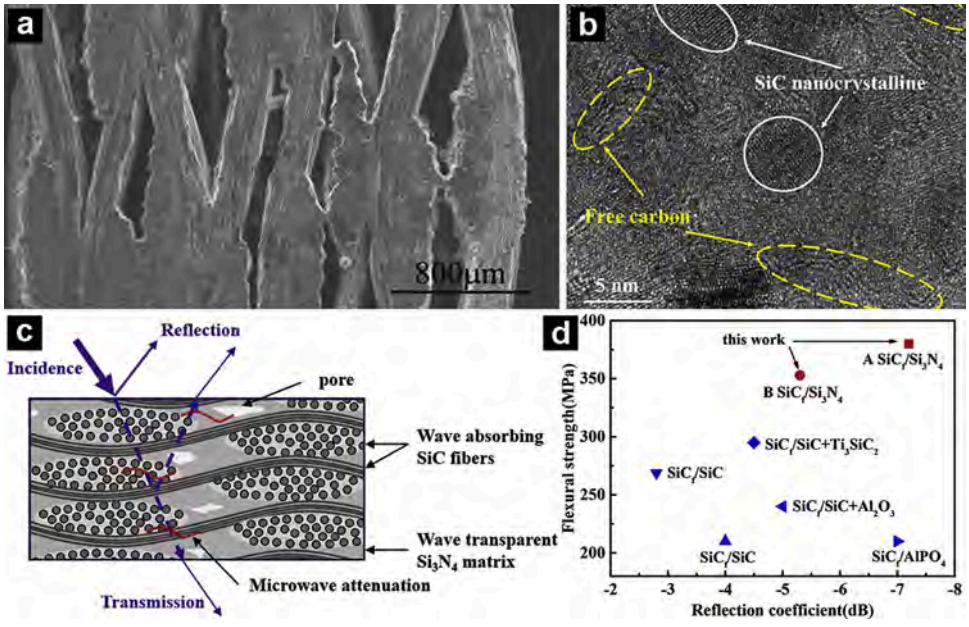

Fig. 12. (a) SEM image (cross-section), (b) TEM image, and (c) EMW absorption mechanism of SiCf/Si_3N_4. (d) Mechanical properties and reflection coefficient of reported ceramic matrix composites. Reproduced with permission [235]. Copyright 2019, Elsevier.

layout. This dramatically enhances the impedance matching of the composite and induces more wave absorption. Second, the grooved structure forms multiple porous holes within the ceramic, enhancing the reflection effect. Based on these reasons, the composite ceramic tends to have a higher wave absorbing ability and higher thermal resistivity than standard SiC/Si_3N_4 composites. This composite was proven to have reliable EMW absorbing performance from 25 °C to 500 °C. Furthermore, anti-oxidation performance is also essential for wave-absorbing ceramics. Because SiC and Si_3N_4 have excellent oxidation resistance, their wave absorbing properties in oxidizing environments are extensively investigated. The Si_3N_4/SiC wire composite was tested at 1200 °C ambient air for several hours [237]. The results showed that after oxidation at 1200 °C for 7.5 h, the complex permittivity either remained the same or decreased a bit. Meanwhile, a dense layer of SiO_2 begins to form, slowing down the diffusion rate of oxygen and preventing further oxidizing effects. These advantages support this Si_3N_4/SiC matrix to maintain high oxidation and high-temperature resistance for small periods.

In a nutshell, combining Si_3N_4 and SiC can drastically increase the impedance matching and thermal resistivity of ceramics. Furthermore, Si_3N_4 and SiC have tunable mechanical structures capable of designing into different layouts, which strongly enhances the wave absorbing abilities. Hence, SiC/Si_3N_4 composites have great application potential in severe environments.

3.5. SiCN-based composite ceramics

SiCN is well known for its unique chemical structure, high thermal and oxidation resistance, and excellent tensile strength. Hence, they are often used as an insulating phase for EMW absorption ceramics, as shown in Table S3 (details in Supplementary Information) [248–286].

3.5.1. SiCN and composites

SiCN is compatible with magnetic and dielectric absorbers. For example, Wang and co-workers developed a polymer-derived SiCN/Fe_2O_3 ceramic via the precursor conversion method [249]. This matrix shows two wave dissipation techniques-polarization loss from the free carbons and magnetic loss from Fe_2O_3. One crucial factor for optimizing wave absorption is to have proper impedance matching, which single-phase dielectric materials often failed to satisfy. However, impedance matching could be easily achieved by this ceramic just by adjusting the content of Fe_2O_3. For this reason, ceramics can maximize its wave absorbing potential, providing a wide EAB from 4~16 GHz. Studies have also found that doping rare earth oxides on SiCN(Fe) can increase the wave absorbing ability of ceramics [262]. For example, Liu et al. coated Dy_2O_3, Eu_2O_3, Sm_2O_3, Y_2O_3, and Gd_2O_3 on SiCN(Fe) ceramic and found the Eu_2O_3 has the best effect. They concluded that the enhancement was probably due to Eu nanoparticles distributed in the matrix, contributing to the rise in the magnetic loss. The analysis shows that the raw SiCN(Fe) has a R_L of −11 dB at 15 GHz, and by doping Eu_2O_3, the minimum R_L can further decrease to −35 dB at 16 GHz. Other magnetic materials like Ni and Co also match well with SiCN-based ceramics. Since the good dielectric property of SiCN ceramics match the magnetic properties of Co_3C particles formed at high temperature, the Co-doped SiCN matrix shows excellent wave absorption performance [282]. Ni is a soft magnetic material with a large saturation magnetization and a high Snoek's limit, exhibiting high permeability and excellent waves absorption [282,283].

Despite having great EMW absorbing ability, magnetic wave absorbers lose their ability at curie temperature. Thus, it is essential to search for alternatives. To address this issue, Long et al. fabricated a Si_3N_4/SiC/SiCN-nanowire composite [257]. The SiCN nanowires have their SiC_xN_y phase distributed in the carbon-rich SiC phase and Si_3N_4 phase, forming multifarious interfacial polarization and relaxation between the SiC_xN_y-SiC interface and SiC_xN_y-Si_3N_4 interface. Meanwhile, the continuous carbon-rich SiC nanowires are beneficial for enhancing conductive loss. As a result, the synergic balance and effect of conductive and polarization loss allow the impedance match of the matrix to be excellent. The SiC nanowires in this experiment were found to have a tensile strength higher than 2 GPa and high-temperature stability up to 1500 °C, validating the potential of ceramic to function in harsh environments. The Si_3N_4/SiC/SiCN composite was reported to have a R_L of −63.7 dB and an EAB of 4.2 GHz.

Besides, Ding et al. synthesized high-temperature resistive MXene-derived TiC/SiBCN ceramics via cross-linking, pyrolysis, and annealing processes (Fig. 13a, b) [265]. MXene was used for its high specific area, outstanding electrical conductivity, and mechanical properties. SiBCN was chosen for its structural stability and high oxidation and thermal resistance. The combination of the two can form a powerful ceramic that can work at temperatures up to 600 °C. When applied to an alternating electric field, positive and negative charges accumulate on the nanograin boundaries, forming an enormous interfacial polarization. Simultaneously, defects in the crystals will cause dipole orientation polarization, and graphite carbons in the ceramic can cause conduction loss (Fig. 13d). Such a wide range of wave dissipating mechanisms balance the complex permittivity and provide excellent impedance matching. The resultant matrix has a R_L of -45.4 dB at 10.9 GHz and bandwidth ranging from 8.4 to 12.4 GHz (Fig. 13c). The SiCN/Al_2O_3 composite prepared by PIP and CVI also shows outstanding mechanical and thermal properties [274]. The traditional PIP or CVI-derived SiCN/Al_2O_3 matrices usually have low complex permittivity and poor EMW absorption during the densification process. Luckily, scientists have found that a combination process of PIP and CVI can sharply shorten the preparation cycle. The periods were found to reach 70 % and 50 % of PIP and CVI processes, respectively. In addition to the short fabricating time, the SiCN/Al_2O_3 composite synthesized by using this method also acquired excellent fracture toughness, flexural strength, temperature resistance, and microwave absorption.

To summarize, doping rare earth oxides or transition metals into SiCN ceramics can achieve larger saturation magnetization and permeability, thereby obtaining good EMW absorption performance. When SiCN is compounded with SiC or Si_3N_4, interfacial polarization and relaxation can be formed, thereby enhancing the conduction loss and obtaining good impedance matching. Importantly, SiCN contributes to the oxidation resistance and thermal stability of the EMW absorber, so the composites can still present considerable EMW absorption performance at high temperature.

3.5.2. SiCN-carbon composites

Like other Si-based ceramics, SiCN-based ceramics are also an excellent match for carbonaceous materials. SiCN can act as the insulating phase that provides better impedance matching and thermal resistance, and carbonaceous materials can perform as conducting phase that increases the electrical conductivity and wave absorption. Although SiCN-carbon composites have not been extensively investigated compared to other Si-carbon composites, current reports show their potential as wave absorbers. Introducing CNW into SiCN is a classic way to improve wave absorption. For instance, Ren et al. fabricated SiCN/CNWs and SiCN/CNWs/SiC hierarchical composites with good wave absorbing ability [259,280]. The results showed that the introduction of CNWs has several benefits compared to other carbonaceous materials like graphene and rGO. First, CNWs have a special one-dimensional structure that processes a relatively low percolation threshold, which favors forming a conductive network in the matrix. Second, the rough surface and abundant defects enhance the polarization effect. Third, its solid polycrystalline structure exhibits lower electrical conductivity than that of rGO and graphene, which benefits the impedance matching. Likewise, CNTs and Cfs also have similar traits to CNWs. Many scientists have proposed different designs. Wang et al. designed a single-walled CNWs/SiCN composite with excellent microwave attenuation capability [255], and Yang et al. synthesized a 3D needled carbon fiber/-SiBCN that sustain thermal stability up to 1000 °C [261], with an

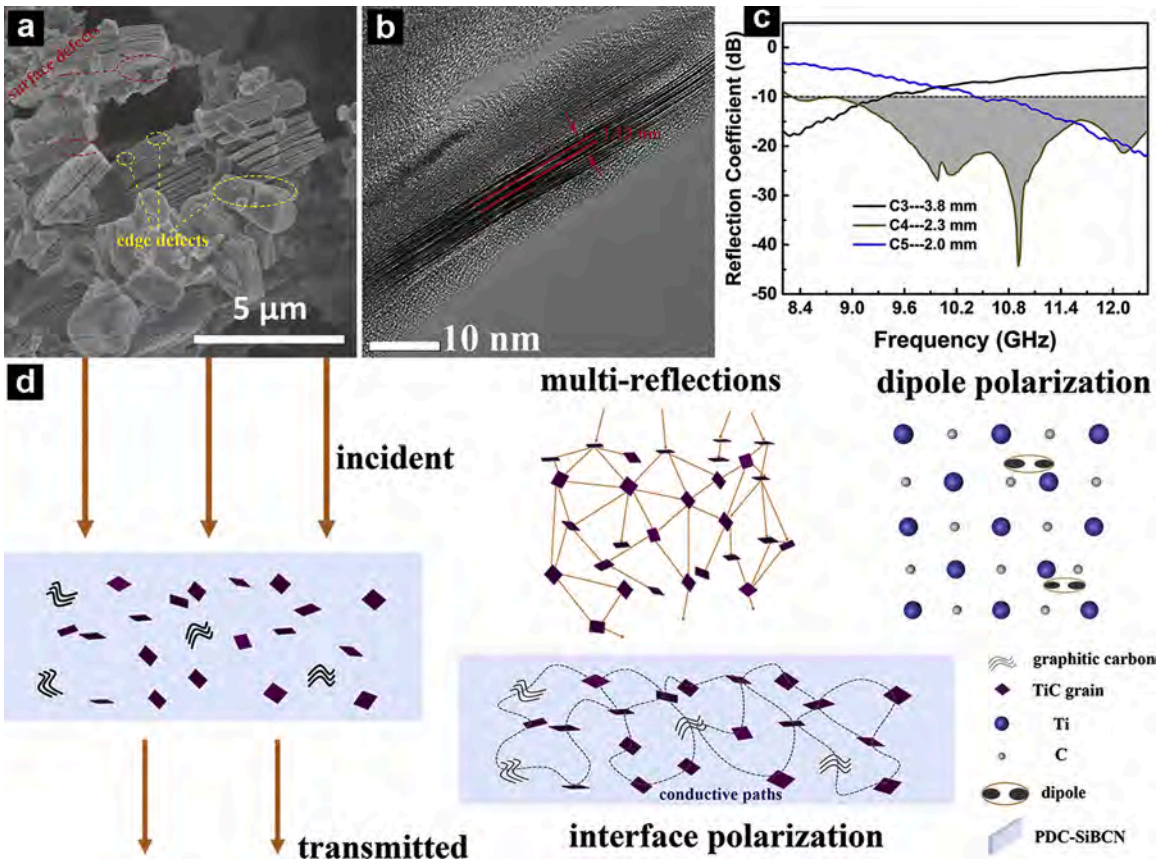

Fig. 13. (a) SEM image, (b) TEM image, (c) R_L value (annealing at different temperatures), and (d) EMW absorption mechanism of MXene-derived TiC/SiBCN ceramic. Reproduced with permission [265]. Copyright 2021, Elsevier.

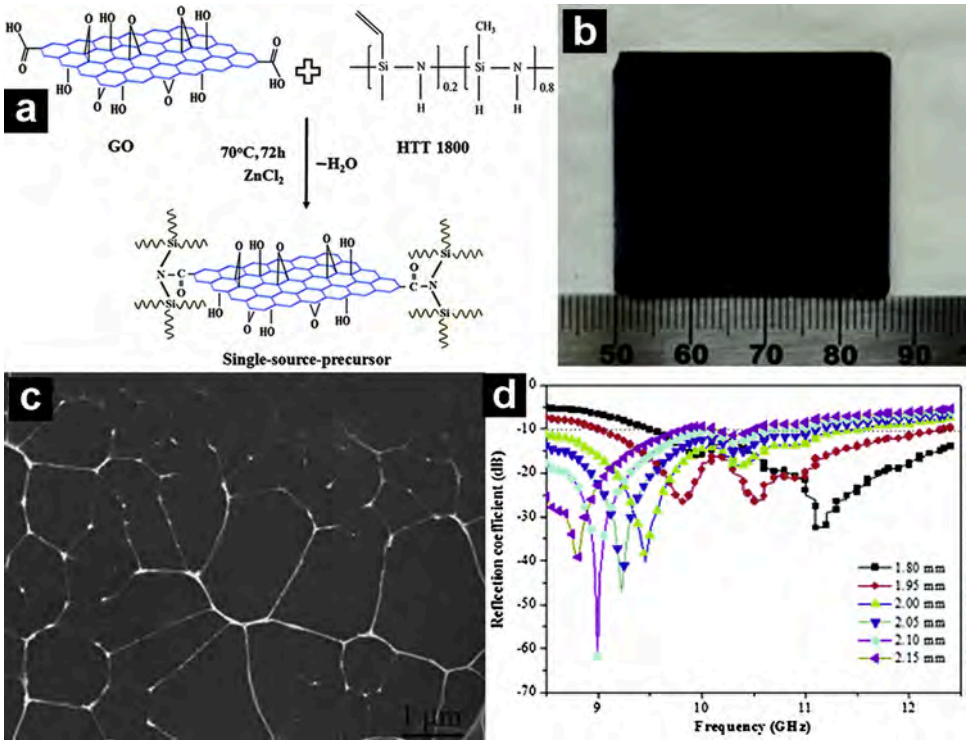

Fig. 14. (a) Scheme showing the synthesis of SSP (GO-HTT 1800). (b) Optical images of monolithic rGO-SiCN composites. (c) SEM image of the fracture surface of rGO-SiCN composites. (d) R_L value (at different thicknesses) of rGO-SiCN composites. Reproduced with permission [271]. Copyright 2017, Royal Society of Chemistry.

outstanding maximum flexural and compression strength of 23.51 ± 1.37 and 12.22 ± 1.12 MPa, respectively.

Moreover, graphene and rGO can also be introduced into SiCN matrice. For instance, Song et al. fabricated the rGO-SiBCN composite by the PDC technique [253]. Graphene is known for its low density, high specific area, and good electrical conductivity. However, its high conductivity often leads to impedance mismatching, making it favors EMW shielding more. To deal with this problem, Song et al. suggested using rGO, which has lower conductivity and better impedance matching. Song et al. then uniformly distributed it in SiBCN, forming multiple conductive networks and extended interfaces. The minimum R_L for this rGO-SiBCN composite was reported to be -34.56 dB, and the EAB was 2.46 GHz in the X-band. In addition, Song also found that this matrix could be further improved by increasing the annealing temperature to 1700 °C. Increasing the annealing temperature expedites the formation of SiC nanocrystals and Si_3N_4 nanowires. SiC nanocrystals benefit wave absorption by generating additional phases for interfacial polarization, while Si_3N_4 nanowires benefit by forming multiple reflections within their aggregated structures. With this adjustment in annealing temperature, the R_L can further decrease to -46.73 dB with an EAB of 3.32 GHz.

One concern about adding carbonaceous materials in SiCN ceramic is that the carbonaceous phase has to be homogeneously distributed in the insulating SiCN phase. Otherwise, the aggregation of the carbon phase will lead to low polarization and poor electrical conductivity, resulting in unsatisfactory EMW absorption. Fortunately, Liu and co-workers came up with a single-source-precursors (SSPs) derived rGO-SiCN composite via an amidation reaction catalyzed by $ZnCl_2$ (Fig. 14a, b) [271]. The SSPs route increases the solubility of GO, hinders GO from restacking, and distributes GO in SiCN evenly (Fig. 14c). The resulting SSPs/rGO-SiCN ceramic mainly consumes waves in two ways. The introduction of uniformly distributed GO significantly increases the conductive loss, and the polarization relaxation induced by the electron motion hysteresis increases the interfacial polarization. With this SSPs technique, the optimal R_L can reach -61.9 dB with an EAB of 3 GHz (Fig. 14d), which is a drastic improvement compared with the physically-blended precursor sample that exhibits an optimal R_L of -8.2 dB. Besides GO, Liu et al. also synthesized a CNT-SiCN ceramic using the SSPs route [270]. With the same CNT content, since a certain amount of CNT is uniformly dispersed in the ceramic matrix, the SSP-derived CNT-SiCN composite has significantly improved EMW absorption properties compared to those from physically-blended-precursors. Therefore, the R_L decreases from -6.4 dB to -21.8 dB with an EAB of 3.7 GHz.

In summary, SiCN-based ceramics are compatible with various types of carbonaceous materials, including CNW, rGO, and graphene. The insulating features of SiCN can help tune impedance matching and supply promising thermal resistance for the matrix. Many research has already proposed powerful combinations that provide satisfactory reflection loss. Foreseeably, more research will be focused on the high-temperature wave absorbing ability of SiCN-carbon composites and their potential applications in military and aerospace engineering.

3.6. Ti_3SiC_2 and composite ceramics

Ti_3SiC_2 is a three-layered ceramic with high electrical conductivity, low density, and high temperature and oxidation resistance. Attributed to these properties, Ti_3SiC_2 can often be used as a promising EMW absorbing material, though that impedance matching has to be carefully controlled due to its high complex permittivity (Table 2).

Zhao and co-workers synthesized Ti_3SiC_2/Al_2O_3 coatings via the plasma spraying process [300]. The layer has a dense structure with Ti_3SiC_2 uniformly distributed in Al_2O_3, in which Al_2O_3 acts as the insulating phase while Ti_3SiC_2 acts as the wave absorbing phase. The matrix mainly dissipates waves by interfacial polarization from Ti_3SiC_2/Al_2O_3 and conductive loss from the Ti_3SiC_2 conductive network. As the content of Ti_3SiC_2 increases, the complex permittivity increases as well due to an increment in interfacial interaction and conductive network. Furthermore, the reflection loss improves but quickly retrogresses after the content of Ti_3SiC_2 reaches 25 wt%. This effect can be described by impedance mismatching, which is strongly related to the relative composition of conductive Ti_3SiC_2 and insulating Al_2O_3. The Ti_3SiC_2/Al_2O_3 coating has a R_L of -24.4 dB at 11.1 GHz and an EAB ranging from 10.1~12.4 GHz. Moreover, the absorber is preferably light, thin, and flexible. Ji et al. recognized this need and fabricated Ti_3SiC_2/poly (TEP, DOP, and PVB) composite films via an inexpensive typecasting process (Fig. 15a) [292]. Like the previous example, this Ti_3SiC_2/poly composite is also sensitive to relative contents. Too much Ti_3SiC_2 can cause aggregation and demolish the flattened film structure. Furthermore, this can also cause impedance matching and regression in tensile strength and Young's modulus (Fig. 15b, c). On the other hand, too little Ti_3SiC_2 will enormously decrease the complex permittivity and deteriorate the wave absorption. Proper regulating the impedance matching allows the heterogeneous interface to form a considerable amount of interfacial polarization (Fig. 15e), while retaining the stretchable, thin, and lightweight characteristics. The optimal film has a R_L of -38.4 dB and an EAB of 2.24 GHz (Fig. 15d).

SiC fibers (SiCf)/mullite (mu) matrices have been widely investigated as a wave absorber ascribed to its excellent mechanical properties and low density. However, the wave absorbing ability of SiCf/mu composites requires improvement. To address this issue, Gao et al. developed a SiCf/mu composite via infiltration and sintering process and reinforced it using hybrid SiC/Ti_3SiC_2 as inert fillers [290]. Given its excellent mechanical properties, adding SiC fillers enhances the flexural strength of the matrix, while adding Ti_3SiC_2 enhances the conductivity loss of the composite. As the content of SiC/Ti_3SiC_2 filler increases, more interfaces will be formed and the polarization relaxation effect will increase. These benefits combined allow the SiCF/mu composite with SiC/Ti_3SiC_2 filler to have excellent mechanical strength, high temperature and oxidation resistance, and excellent reflection loss. The reported R_L of this matrix is -53 dB at 8.64 GHz, with the EAB ranging from 9 to 12.3 GHz. In addition, Ti_3SiC_2 can also form composites with magnetic materials. For instance, Garg and co-workers synthesized $SrFe_{12}O_{19}$/-Ti_3SiC_2 powder with dielectric and magnetic loss mechanisms [291].

Table 2
Reported Ti_3SiC_2 and composite ceramics for EMW absorption.

Materials	Shapes	Methods	R_L and thickness	Ref.
Ti_3SiC_2	Foams	Pre-frozen	−50.6 dB, 1.8 mm	[287]
MXene/FeCo	Films	Electrostatic interaction	−43.7 dB, 2.0 mm	[288]
Cordierite/Ti_3SiC_2	Grains	Hot-pressed sintering	−16.4 dB, 1.6 mm	[289]
SiC/mullite/Ti_3SiC_2	Fibers	Infiltration and sintering	−53.0 dB, 2.9 mm	[290]
$SrFe_{12}O_{19}/Ti_3SiC_2$	Grains	Autocombustion and PIP	−39.7 dB, 2.0 mm	[291]
Ti_3SiC_2/poly(TEP, DOP, and PVB)	Layer	Casting process	−38.4 dB, 1.6 mm	[292]
Al_2O_3/Ti_3SiC_2	Grains	Hot-pressed sintering	−20.0 dB, 2.2 mm	[293]
Cordierite/Ti_3SiC_2	Grains	Hot-pressed sintering	−16.4 dB, 1.6 mm	[294]
Cordierite/Ti_3SiC_2	Grains	Hot-pressed sintering	−24.0 dB, 1.6 mm	[295]
SiO_2/Ti_3SiC_2	Grains	Stober route, heat-treated	−15.0 dB, 2.4 mm	[296]
Ti_3SiC_2/Cu/epoxy resin	Grains	Electroless plating	−37.0 dB, 1.8 mm	[297]
Cordierite/Ti_3SiC_2	Grains	Plasma spraying	−49.3 dB, 1.5 mm	[298]
Glass/Ti_3SiC_2	Grains	Plasma spraying	−47.7 dB, 1.4 mm	[299]
Al_2O_3/Ti_3SiC_2	Grains	Plasma spraying	−24.4 dB, 1.3 mm	[300]

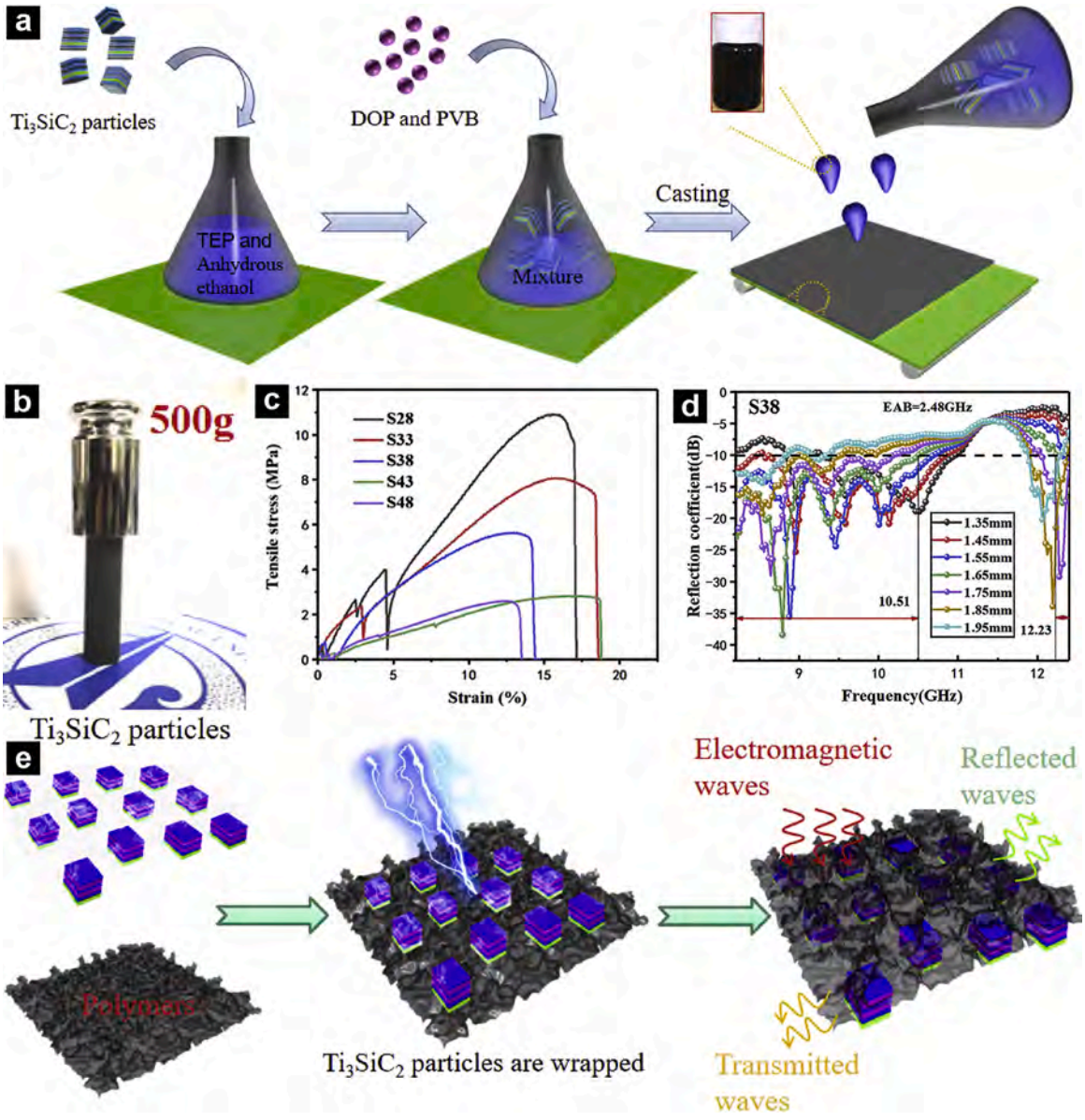

Fig. 15. (a) Scheme showing the synthetic process of Ti_3SiC_2-based films by tape casting. (b) The Ti_3SiC_2-based film can support ~170 times its own weight. (c) Stress-strain curves for Ti_3SiC_2-based film with different Ti_3SiC_2 contents. (d) R_L value (at different thicknesses) and (e) EMW absorption mechanism for Ti_3SiC_2/poly composite. Reproduced with permission [292]. Copyright 2020, Elsevier.

The composite shows remarkable improvement in reflection loss compared to pure $SrFe_{12}O_{19}$ and Ti_3SiC_2. This is mainly because the unique structure of $SrFe_{12}O_{19}$ and Ti_3SiC_2 allows them to mix homogeneously and form better impedance matching between magnetic and dielectric materials. The optimal result was obtained when the matrix contains 20 % Ti_3SiC_2 and 80 % $SrFe_{12}O_{19}$. The R_L of -39.67 dB is observed at 9.46 GHz, and the EAB is 2.77 GHz.

High temperature and oxidation resistance are also important traits of Ti_3SiC_2 composites. Several studies have proved that Ti_3SiC_2/cordierite composites were promising wave absorbers with superb heat resistance [289,295,298]. The Ti_3SiC_2/cordierite matrix is usually fabricated by milling the Ti_3SiC_2 powder and introducing them into the insulating cordierite matrix through hot-pressed sintering. Reports showed that when Ti_3SiC_2/cordierite was oxidized at 800~1000 °C [295], the complex permittivity of the ceramic decreased accordingly due to the reduction of Ti_3SiC_2 content. However, the low permittivity oxidation products TiO_2 and SiO_2 formed on the surface are beneficial for the entrance of EMW, which helps the ceramic to retain a satisfactory state after 60 h of high-temperature oxidation. Another high-temperature resistive composite is SiO_2 coated Ti_3SiC_2 [296]. Since SiO_2 is an insulating material, it hinders the polarization and electric conductive loss of Ti_3SiC_2. In addition, the insulating SiO_2 layer will seriously hinder the hopping of free electrons, thereby destroying the formation of the conductive network. Nevertheless, it endows a protective layer for the composite to resist oxidation and high temperature. Therefore, due to the SiO_2 protective layer, SiO_2/Ti_3SiC_2 exhibits better wave absorption properties than bare Ti_3SiC_2 powder after oxidation at 600 °C.

Conclusively, as a new type of ceramic material, layered MXene (Ti_3SiC_2) ceramics has high electrical conductivity, which enables high complex permittivity. Furthermore, the workability of layered MXene makes it have good mechanical flexibility. MXene can also be compounded with a variety of materials to obtain suitable impedance matching and good EMW absorption performance. In addition, MXene also has high temperature and oxidation resistance, even after oxidation at 600 °C, it still delivers prominent EMW absorption performance.

4. Summary and outlook

In this review, we have summarized the recent process in the design principles and strategies of silica-based ceramics toward EMW absorption in terms of the structure and component design, and we have provided the mechanism of interfacial polarization, dipole polarization, conduction loss, Eddy current loss, natural resonance, and multiple reflection/scattering for different EMW absorbers. By adjusting the element type, ratio, and structure of the second/third component (dielectric material) in silica-based ceramics (SiO_2, SiOC, SiC, SiCN, Si_3N_4), the thermal stability, as well as oxidation resistance of the composite, can be improved, and the working range can be expanded, especially in high-temperature environments. Moreover, the dielectric component can regulate the dielectric properties and dielectric loss to obtain a good impedance matching with magnetic loss, providing considerable reflection loss. In addition to the component design in silica-based ceramics, structural design such as creating novel nanostructures (e.g. porous, hollow, core-shell, multi-layer, and hierarchical) to endow them scattering and multiple reflection capabilities and improve the transmission path of electromagnetic waves can also enhance the EMW absorption properties of silica-based ceramics. Furthermore, the construction of multi-interface silica-based ceramics may produce more striking results because it can potentially bring charge polarization and interfacial polarization with the associated relaxation, and improve the overall EMW absorption properties. By studying the influence of different conditions on the component and structure of silica-based ceramics, the magnetic loss and dielectric loss under ideal reaction conditions were revealed, resulting in a deep understanding of the EMW absorption mechanism. Fully reveal these design principles and mechanisms, and provide clues for researchers to construct high-performance silica-based ceramics EMW absorbers.

Despite major advances in designing high-performance silica-based ceramics EMW absorbers, there are still many basic open issues and obstacles to be overcome in the following aspects.

(1) In practical application, the density, thickness, and cost of EMW absorbers are the important indicators to judge whether absorbers can be applied [301–304]. However, the structure of ceramic materials is dense and large in weight. At present, many silica-based ceramics are prepared into nanostructures (nanocrystal, nanosphere, nanofiber, nanowire, nanotube, nanosheet, 3D foam) to increase the specific surface area and the transmission path of electromagnetic waves [305–311], thereby deliver lightweight and high reflection loss characteristics. Meanwhile, the high sintering temperature and long sintering time of ceramic materials make the preparation very high. Recently, some fast heating techniques (liquid phase sintering, fast-firing sintering) and modern sintering techniques (field-assisted sintering technology, pressure-assisted sintering, temperature stage controlled sintering) have been further developed to promote the densification of grain growth [78–82]. Consequently, the sintering temperature and time can be significantly reduced, so that energy consumption is relatively low. This may be an effective way for the rapid establishment of updated industrial EMW absorbers.

(2) Research on theoretical silica-based ceramic models is necessary to reveal the relationship between structure and performance. Although the research on EMW absorption mechanism in some silica-based ceramic models has been very mature, advanced operational insights into some EMW absorption processes, especially EMW absorption under high-temperature conditions [23, 125,312,313], are still needed to develop effective strategies to maintain the optimal EMW absorption state. For instance, in a continuously changing temperature environment, the structure of ceramic materials may also change as well as the varied EMW absorption performance, but there is still a lack of *in-situ* testing methods in this regard. In addition, precisely customize the structure and composition, and the reaction system (temperature, time, pH value, atmosphere) are the critical factors to accurately achieve the high-performance EMW absorption performance. Finally, it is necessary to explore the instrumental (dedicated *in-situ* chamber, high time resolution for rapid testing) and experimental parts for operando research through FTIR, Raman, XRD, or XAFS methods.

(3) Another issue for the silica-based ceramic EMW absorber appears in the mechanism research, which is not comprehensive. Even though the multi-layer or hierarchical nanostructures of silica-based ceramics or their combination with dielectric materials were demonstrated to be favorable for generating multiple reflections and improving impedance matching [314–317], the intrinsic mechanisms remain unclear. What is the ideal layer number or pore size range of silica-based ceramics for EMW absorption? How does it affect the multiple reflections and scattering? Various theoretical calculations (such as DFT, Ansys) and experiments (such as *in-situ* FTIR, Raman, TEM) are used to determine active sites in catalysis [318–322]. These advanced methods should also be accurately applied to the field of EMW absorption to further identify the EMW absorption mechanism.

(4) Finally, as mentioned above, the developed EMW absorbers need to meet the characteristics of lightweight (thin thickness), wide effective absorption width, and high reflection loss. It can be expected that the design of ultrathin thickness (<1 mm), ultrawide EAB (>10 GHz, R_L <−10 dB), and high efficient EMW absorbers will be the main direction of future research, especially in the face of the ever-increasing demand for upsizing and a lightness of device [323–325]. In addition, most of the current EMW absorption materials can effectively absorb the centimeter wave (8−18 GHz). However, with the development of meter-wave and millimeter-wave military radar technology, EMW absorption materials should be compatible with meter waves, centimeter waves, and even infrared and lasers. Therefore, the design of silica-based ceramics for multi-band EMW absorption will become an important research trend. Nevertheless, the design and preparation of multi-component and novel nanostructured silica-based ceramic materials with high-performance EMW absorption capabilities will contribute to this aspect.

Summary of novel conclusions

Nevertheless, comprehensive information on silicon-based ceramic and electromagnetic microwave (EMW) absorption materials is scarce, although much excellent progress has been made in this field. In this review, we have summarized the recent process in the design principles and strategies of silica-based ceramics toward EMW absorption in terms of the structure and component design, and we have provided the mechanism of interfacial polarization, dipole polarization, conduction loss, Eddy current loss, natural resonance, and multiple reflection/scattering for different EMW absorbers. By adjusting the element type, ratio, and structure of the second/third component (dielectric material) in silica-based ceramics (SiO2, SiOC, SiC, SiCN, Si3N4), the thermal stability, as well as oxidation resistance of the composite, can be improved, and the working range can be expanded, especially in high-temperature environments. Moreover, the dielectric component can regulate the dielectric properties and dielectric loss to obtain a good impedance matching with magnetic loss, providing considerable reflection loss. In addition to the component design in silica-based ceramics, structural design such as creating novel nanostructures (e.g. porous, hollow, core-shell, multi-layer, and hierarchical) to endow them scattering and multiple reflection capabilities and improve the transmission path of electromagnetic waves can also enhance the EMW absorption properties of silicabased ceramics. Furthermore, the construction of multi-interface silica-based ceramics may produce more

striking results because it can potentially bring charge polarization and interfacial polarization with the associated relaxation, and improve the overall EMW absorption properties. By studying the influence of different conditions on the component and structure of silica-based ceramics, the magnetic loss and dielectric loss under ideal reaction conditions were revealed, resulting in a deep understanding of the EMW absorption mechanism. Fully reveal these design principles and mechanisms, and provide clues for researchers to construct high-performance silica-based ceramics EMW absorbers.

Declaration of Competing Interest

The authors declare that they have no known competing financial interests or personal relationships that could have appeared to influence the work reported in this paper.

Acknowledgement

This work was supported by the National Natural Science Foundation of China under Grant nos. 51671010 and 51101007.

Appendix A. Supplementary data

Supplementary material related to this article can be found, in the online version, at doi:https://doi.org/10.1016/j.jeurceramsoc.2021.08.009.

References

[1] Y. Li, X.F. Liu, X.Y. Nie, W.W. Yang, Y.D. Wang, R.H. Yu, J.L. Shui, Adv. Funct. Mater. 29 (2019), 1807624.
[2] Q. Li, Z. Zhang, L.P. Qi, Q.L. Liao, Z. Kang, Y. Zhang, Adv. Sci. 6 (2019), 1801057.
[3] M.K. Han, Y.Q. Liu, R. Rakhmanov, C. Israel, M.A.S. Tajin, G. Friedman, V. Volman, A. Hoorfar, K.R. Dandekar, Y. Gogotsi, Adv. Mater. 33 (2021), 2003225.
[4] X.J. Zeng, G.M. Jiang, L.Y. Zhu, C.Y. Wang, M. Chen, R.H. Yu, ACS Appl. Nano Mater. 2 (2019) 5475–5482.
[5] Z.Y. Huang, H.H. Chen, Y. Huang, Z. Ge, Y. Zhou, Y. Yang, P.S. Xiao, J.J. Liang, T. F. Zhang, Q. Shi, G.H. Li, Y.S. Chen, Adv. Funct. Mater. 28 (2018), 1704363.
[6] Y.Y. Zhu, J. Liu, T. Guo, J.J. Wang, X.Z. Tang, V. Nicolosi, ACS Nano 15 (2021) 1465–1474.
[7] X.J. Zeng, L.Y. Zhu, B. Yang, R.H. Yu, Mater. Des. 189 (2020), 108517.
[8] M.S. Cao, X.X. Wang, M. Zhang, W.Q. Cao, X.Y. Fang, J. Yuan, Adv. Mater. 32 (2020), 1907156.
[9] X.J. Zeng, X.Y. Cheng, R.H. Yu, G.D. Stucky, Carbon 168 (2020) 606–623.
[10] Y.H. Lu, S.L. Zhang, M.Y. He, L. Wei, Y. Chen, R.N. Liu, Carbon 178 (2021) 413–435.
[11] R.L. Yang, X.C. Gui, L. Yao, Q.M. Hu, L.L. Yang, H. Zhang, Y.T. Yao, H. Mei, Z. K. Tang, Nano-Micro Lett. 13 (2021) 66.
[12] B. Quan, W.H. Shi, S.J.H. Ong, X.C. Lu, P.L. Wang, G.B. Ji, Y.F. Guo, L.R. Zheng, Z.C.J. Xu, Adv. Funct. Mater. 29 (2019), 1901236.
[13] H.L. Lv, Z.H. Yang, S. Jun, H. Ong, C. Wei, H.B. Liao, S.B. Xi, Y.H. Du, G.B. Ji, Z.C. J. Xu, Adv. Funct. Mater. 29 (2019), 1900163.
[14] L.L. Yan, M. Zhang, S.C. Zhao, T.J. Sun, B. Zhang, M.S. Cao, Y. Qin, Chem. Eng. J. 382 (2020), 122860.
[15] F. Wang, C. Bai, L. Chen, Y. Yu, Mater. Today Nano 13 (2021), 100108.
[16] F. Pan, L.Z. Yu, Z. Xiang, Z.C. Liu, B.W. Deng, E.B. Cui, Z. Shi, X. Li, W. Lu, Carbon 172 (2021) 506–515.
[17] H.H. Zhao, X.Z. Xu, Y.H. Wang, D.G. Fan, D.W. Liu, K.F. Lin, P. Xu, X.J. Han, Y. C. Du, Small 16 (2020), 2003407.
[18] J. Qiao, X. Zhang, C. Liu, L.F. Lyu, Y.F. Yang, Z. Wang, L.L. Wu, W. Liu, F.L. Wang, J.R. Liu, Nano-Micro Lett. 13 (2021) 75.
[19] X.H. Liang, Z.M. Man, B. Quan, J. Zheng, W.H. Gu, Z. Zhang, G.B. Ji, Nano-Micro Lett. 12 (2020) 102.
[20] B. Aïssa, A. Sinopoli, A. Ali, Y. Zakaria, A. Zekri, M. Helal, M. Nedil, F. Rosei, S. Mansour, K.A. Mahmoud, Carbon 173 (2021) 528–6539.
[21] Ce Cui, R.H. Guo, E.H. Ren, H.Y. Xiao, M. Zhou, X.X. Lai, Q. Qin, S.X. Jiang, W. F. Qin, Chem. Eng. J. 405 (2021), 126626.
[22] Y.J. Wan, K. Rajavel, X.M. Li, X.Y. Wang, S.Y. Liao, Z.Q. Lin, P.L. Zhu, R. Sun, C. P. Wong, Chem. Eng. J. 408 (2021), 127303.
[23] D.W. Hu, S.Q. Wang, C. Zhang, P.S. Yi, P.K. Jiang, X.Y. Huang, Nano Res. 17 (2021) 2837–2845.
[24] C.B. Liang, H. Qiu, P. Song, X.T. Shi, J. Kong, J.W. Gu, Sci. Bull. 65 (2020) 616–622.
[25] Y. Xiong, L.L. Xu, C.X. Yang, Q.F. Sun, X.J. Xu, J. Mater. Chem. A 8 (2020) 18863–18871.
[26] Z.L. Ma, S.L. Kang, J.Z. Ma, L. Shao, Y.L. Zhang, C. Liu, A.J. Wei, X.L. Xiang, L. F. Wei, J.W. Gu, ACS Nano 14 (2020) 8368–8382.
[27] X.Y. Yuan, R.Q. Wang, W.R. Huang, L. Kong, S.W. Guo, L.F. Cheng, ACS Appl. Mater. Interfaces 12 (2020) 13208–13216.
[28] X.X. Wang, W.Q. Cao, M.S. Cao, J. Yuan, Adv. Mater. 32 (2020), 2002112.
[29] Q. Song, F. Ye, L. Kong, Q.L. Shen, L.Y. Han, L. Feng, G.J. Yu, Y.A. Pan, H.J. Li, Adv. Funct. Mater. 30 (2020), 2000475.
[30] G.B. Sun, B.X. Dong, M.H. Cao, B.Q. Wei, C.W. Hu, Chem. Mater. 23 (2011) 1587–1593.
[31] M. Green, X.B. Chen, J. Materiomics 5 (2019) 503–541.
[32] U.S. Congress, New Structural Materials Technologies: Opportunities for the use of Advanced Ceramics and Composites-a Technical Memorandum, Office of Technology Assessment. OTA-TM-E-32, US Government Printing Office, Washington DC, USA, 1986.
[33] Z.-Y. Shen, Y. Wang, Y.X. Tang, Y.Y. Yu, W.-Q. Luo, X.C. Wang, Y.M. Li, Z. M. Wang, F.S. Song, J. Materiomics 5 (2019) 641–648.
[34] P. Colombo, Philos. Trans. R. Soc. A 364 (2006) 109–124.
[35] A.R. Studart, U.T. Gonzenbach, E. Tervoort, L.J. Gauckler, J. Am. Ceram. Soc. 89 (2006) 1771–1789.
[36] W.T. Cao, F.F. Chen, Y.J. Zhu, Y.G. Zhang, Y.Y. Jiang, M.G. Ma, F. Chen, ACS Nano 12 (2018) 4583–4593.
[37] Y. Zhang, Y. Huang, T.F. Zhang, H.C. Chang, P.S. Xiao, H.H. Chen, Z.Y. Huang, Y. S. Chen, Adv. Mater. 27 (2015) 2049–2053.
[38] W.L. Song, X.T. Guan, L.Z. Fan, Y.B. Zhao, W.Q. Cao, C.Y. Wang, M.S. Cao, Carbon 100 (2016) 109–117.
[39] J.T. Feng, Y.H. Hou, Y.C. Wang, L.C. Li, ACS Appl. Mater. Interfaces 9 (2017) 14103–14111.
[40] Q.H. Liu, Q. Cao, H. Bi, C.Y. Liang, K.P. Yuan, W. She, Y.J. Yang, R.C. Che, Adv. Mater. 28 (2016) 486–490.
[41] W.H. Huang, X.X. Zhang, Y.N. Zhao, J. Zhang, P.B. Liu, Carbon 167 (2020) 19–30.
[42] X.J. Zeng, L.Y. Zhu, G.M. Jiang, C.Y. Wang, Z.H. Xia, R.H. Yu, Phys. Status Solidi A 215 (2018), 1701049.
[43] L.J. Yu, Q.X. Yang, J.L. Liao, Y.F. Zhu, X. Li, W.T. Yang, Y.Q. Fu, Chem. Eng. J. 352 (2018) 490–500.
[44] X.J. Zeng, B. Yang, H.Z. Yang, L.Y. Zhu, R.H. Yu, AIP Adv. 7 (2017), 056605.
[45] S. Affatato, R. Alessandro, M. Massimiliano, Compos. Part B-Eng. 83 (2015) 276–283.
[46] A.N. Samant, N.B. Dahotre, J. Eur. Ceram. Soc. 29 (2009) 969–993.
[47] A. Sommers, Q. Wang, X. Han, C. T'Joen, Y. Park, A. Jacobi, Appl. Therm. Eng. 30 (2010) 1277–1291.
[48] S. Affatato, M. Testoni, G.L. Cacciari, A. Toni, Biomaterials 20 (1999) 971–975.
[49] X.Y. Li, K. Lu, Nat. Mater. 16 (2017) 700–701.
[50] S. Tammas-Williams, I. Todd, Scripta Mater. 135 (2017) 105–110.
[51] K.D. Vogiatzis, M.V. Polynski, J.K. Kirkland, J. Townsend, A. Hashemi, C. Liu, E. A. Pidko, Chem. Rev. 119 (2019) 2453–2523.
[52] G.A. Filonenko, R. van Putten, E.J.M. Hensen, E.A. Pidko, Chem. Soc. Rev. 47 (2018) 1459–1483.
[53] A. Vyatskikh, S. Delalande, A. Kudo, X. Zhang, C.M. Portela, J.R. Greer, Nat. Commun. 9 (2018) 593.
[54] H. Kargarzadeh, J. Huang, N. Lin, I. Ahmad, M. Mariano, A. Dufresne, S. Thomas, A. Gałęski, Prog. Polym. Sci. 87 (2018) 197–227.
[55] S.D. Kang, G.J. Snyder, Nat. Mater. 16 (2017) 252–257.
[56] N. Chaoui, M. Trunk, R. Dawson, J. Schmidt, A. Thomas, Chem. Soc. Rev. 46 (2017) 3302–3321.
[57] S.C. Ligon, R. Liska, J. Stampfl, M. Gurr, R. Mülhaupt, Chem. Rev. 117 (2017) 10212–10290.
[58] M.G.T.A. Rutten, F.W. Vaandrager, J.A.A.W. Elemans, R.J.M. Nolte, Nat. Rev. Chem. 2 (2018) 365–381.
[59] Y.H. Cai, L.J. Huo, Y.M. Sun, Adv. Mater. 29 (2017), 1605437.
[60] M. Belmonte, Adv. Eng. Mater. 8 (2006) 693–703.
[61] D.W. Richerson, Modern Ceramic Engineering: Properties, Processing, and use in Design, CRC press, 2005.
[62] R.J. Zeng, S.X. Gao, Overview of fine ceramic industry in Fujian, China Ceram. Ind. 1 (2009).
[63] A.L. Giudice, C. Ingrao, M.T. Clasadonte, C. Tricase, C. Mbohwa, J. Clean. Prod. 142 (2017) 225–239.
[64] W.-D. Emmerich, J. Hayhurst, E. Kaisersberger, Thermochim. Acta 106 (1986) 71–78.
[65] A.G. Evans, T.G. Langdon, Prog. Mater. Sci. 21 (1976) 171–285.
[66] I.J. McColm, Special Ceramics for Modern Applications: Which? Why? How? Ceramic Processing, Springer, Dordrecht, 1995, pp. 1–33.
[67] I.P. Tuersley, A. Jawaid, I.R. Pashby, J. Mater. Process. Technol. 42 (1994) 3773–3790.
[68] S.H. Yu, J. Ceram. Soc. Jpn. 109 (2001) S65–S75.
[69] M. Bengisu, Engineering Ceramics, Springer Science & Business Media, 2013.
[70] R.K. Nishihora, P.L. Rachadel, M.G.N. Quadri, D. Hotza, J. Eur. Ceram. Soc. 38 (2018) 988–1001.
[71] S. Deville, Adv. Eng. Mater. 10 (2008) 155–169.
[72] J. González-Gutiérrez, G.B. Stringari, I. Emri, Powder injection molding of metal and ceramic parts. Some Critical Issues for Injection Molding, 2012, pp. 65–88.
[73] Z.W. Chen, Z.Y. Li, J.J. Li, C.B. Liu, C.S. Lao, Y.L. Fu, C.Y. Liu, Y. Li, P. Wang, Y. He, J. Eur. Ceram. Soc. 39 (2019) 661–687.
[74] L.L. Yang, X.J. Zeng, Y. Zhang, Mater. Lett. 255 (2019), 126564.
[75] L.L. Yang, X.J. Zeng, A. Ditta, B. Feng, L.Z. Su, Y. Zhang, J. Adv. Ceram. 9 (2020) 312–319.

[76] M. Singh, H.M. Haverinen, P. Dhagat, G.E. Jabbour, Adv. Mater. 22 (2010) 673–685.
[77] S.A. Skoog, P.L. Goering, R.J. Narayan, J. Mater. Sci. Mater. Med. 25 (2014) 845–856.
[78] H.Q. Lian, X.M. Yao, Z.R. Huang, Y.P. Zeng, B.Z. Su, J. Eur. Ceram. Soc. 36 (2016) 1863–1871.
[79] D.S.B. Heidary, M. Lanagan, C.A. Randall, J. Eur. Ceram. Soc. 38 (2018) 1018–1029.
[80] S.K. Jha, X.L. Phuah, J. Luo, C.P. Grigoropoulos, H.Y. Wang, E. García, B. Reeja-Jayan, J. Am. Ceram. Soc. 102 (2019) 5–31.
[81] R. Chaim, G. Chevallier, A. Weibel, C. Estournès, J. Mater. Sci. 53 (2018) 3087–3105.
[82] H.B. Yang, L. Li, Y.Y. Li, B. Shen, Y.M. Kang, L.B. Zhao, J.J. Li, Y.H. Dong, J.G. Li, J. Materiomics 7 (2021) 837–844.
[83] C.A. Randall, J. Guo, A.L. Baker, M.T. Lanagan, H.Z. Guo, Cold Sintering Ceramics and Composites, US Provisional Patent Application 15/277, 553, 2017.
[84] H.Z. Guo, A.L. Baker, J. Guo, C.A. Randall, J. Am. Ceram. Soc. 99 (2016) 3489–3507.
[85] J. Guo, H.Z. Guo, A.L. Baker, M.T. Lanagan, E.R. Kupp, G.L. Messing, C. A. Randall, Angew. Chem. Int. Ed. 55 (2016) 11457–11461.
[86] H.Z. Guo, A.L. Baker, J. Guo, C.A. Randall, ACS Nano 10 (2016) 10606–10614.
[87] H.Z. Guo, J. Guo, A.L. Baker, C.A. Randall, J. Am. Ceram. Soc. 100 (2017) 491–495.
[88] C. Vakifahmetoglu, L. Karacasulu, Curr. Opin. Solid State Mater. Sci. 24 (2020), 100807.
[89] C.W. Wang, W.W. Ping, Q. Bai, H.C. Cui, R. Hensleigh, R.L. Wang, A.H. Brozena, Z.P. Xu, J.Q. Dai, Y. Pei, C.L. Zheng, G. Paste, J.L. Gao, X.Z. Wang, H. Wang, J.-C. Zhao, B. Yang, X.Y. Zheng, J. Luo, Y.F. Mo, B. Dunn, L.B. Hu, Science 368 (2020) 521–526.
[90] A. Harrati, A. Manni, A.E. Bouari, I.-E.E.A. EI Hassani, C. Sadik, Mater. Today: Proc. 30 (2020) 876–882.
[91] G.R. Faseeva, R.M. Nafikov, S.E. Lapuk, Yu.A. Zakharov, A.A. Novik, A. A. Vjuginova, R.R. Kabirov, L.N. Garipov, Ceram. Int. 43 (2017) 7202–7210.
[92] X.F. Liu, L.Y. Xiao, Y. Zhang, H.J. Sun, J. Materiomics 6 (2020) 256–262.
[93] P. Singh, G. Kaur, K. Singh, B. Singh, M. Kaur, M. Kaur, U. Krishnan, M. Kumar, R. Bala, A. Kumar, Appl. Nanosci. 8 (2018) 1–9.
[94] A. Celebanska, M. Opallo, ChemElectroChem 3 (2016) 1629–1634.
[95] S. Verma, S. Sinha-Ray, S. Sinha-Ray, Polymers 12 (2020) 238.
[96] Z.H. Li, S.T. Liu, S.G. Song, W.L. Xu, Y.M. Sun, Y.Q. Dai, Compos. Commun. 15 (2019) 168–178.
[97] X.J. Zeng, X.D. Hu, H.B. Song, G.H. Xia, Z.-Y. Shen, R.H. Yu, M. Moskovits, Microporous Mesoporous Mater. 323 (2021), 111262.
[98] D.X. Li, Z.-Y. Shen, Z.P. Li, W.Q. Luo, F.S. Song, X.C. Wang, Z.M. Wang, Y.M. Li, J. Mater. Chem. C 8 (2020) 7650–7657.
[99] P. Dutta, A. Sikdar, A. Majumdar, M. Borah, N. Padma, S. Ghosh, U.N. Mait, Carbon 169 (2020) 225–234.
[100] X. Wang, H.W. Zhai, B.Y. Qie, Q. Cheng, A.J. Li, J. Borovilas, B.Q. Xu, C.M. Shi, T. W. Jin, X.B. Liao, Y.B. Li, X.D. He, S.Y. Du, Y.K. Fu, M. Dontigny, K. Zaghib, Y. Yang, Nano Energy 60 (2019) 205–212.
[101] Y. Zhao, J.H. Yan, W.P. Cai, Y.M. Lai, J. Song, J.Y. Yu, B. Ding, Energy Storage Mater. 23 (2019) 306–313.
[102] G. Chen, J. Chen, W.J. Pei, Y.M. Lu, Q.F. Zhang, Q. Zhang, Y.B. He, Mater. Res. Bull. 110 (2019) 39–49.
[103] D.X. Li, Z.-Y. Shen, Z.P. Li, W.Q. Luo, X.C. Wang, Z.M. Wang, F.S. Song, Y.M. Li, J. Adv. Ceram. 9 (2020) 183–192.
[104] K. Bae, D.H. Kim, H.J. Choi, J.-W. Son, J.H. Shim, Adv. Energy Mater. 8 (2018), 1801315.
[105] X.J. Zeng, J.L. Shui, X.F. Liu, Q.T. Liu, Y.C. Li, J.X. Shang, L.R. Zheng, R.H. Yu, Adv. Energy Mater. 8 (2018), 1701345.
[106] D.X. Li, X.J. Zeng, Z.P. Li, Z.-Y. Shen, H. Hao, W.Q. Luo, X.C. Wang, F.S. Song, Z. M. Wang, Y.M. Li, J. Adv. Ceram. 10 (2021) 675–703.
[107] C.S. Jiang, N. Dunlap, Y.J. Li, H. Guthrey, P. Liu, S.-H. Lee, M.M. Al-Jassim, Adv. Energy Mater. 10 (2020), 2000219.
[108] Z.L. Cheng, F. Ye, Y.S. Liu, T.L. Qiao, J.P. Li, H.L. Qin, L.F. Cheng, L.T. Zhang, J. Adv. Ceram. 8 (2019) 399–407.
[109] L.L. Shu, R.H. Liang, Z.G. Rao, L.F. Fei, S.M. Ke, Y. Wang, J. Adv. Ceram. 8 (2019) 153–173.
[110] V.T. Rathod, J.S. Kumar, A. Jain, Appl. Nanosci. 7 (2017) 519–548.
[111] T. Li, T.M.M. Heenan, M.F. Rabuni, B. Wang, N.M. Farandos, G.H. Kelsall, D. Matras, C. Tan, X.K. Lu, S.D.M. Jacques, D.J.L. Brett, P.R. Shearing, M. D. Michiel, A.M. Beale, A. Vamvakeros, K. Li, Nano Lett. 20 (2020) 3828–3835.
[112] Y. Nakamura, Y. Sakai, M. Azuma, S.-i. Ohkoshi, Sci. Adv. 6 (2020) eaaz5264.
[113] W.L. Huo, X.Y. Zhang, E. Tervoort, S. Gantenbein, J.L. Yang, A.R. Studart, Adv. Funct. Mater. (2020), 2003550.
[114] C. Jia, L. Li, Y. Liu, B. Fang, H. Ding, J.N. Song, Y.B. Liu, K.J. Xiang, S. Lin, Z. W. Li, W.J. Si, B. Li, X. Shen, D.Z. Wang, X.D. Wei, H. Wu, Nat. Commun. 11 (2020) 3732.
[115] F.S. Li, H.W. Zhao, Y.H. Yue, Z. Yang, Y.W. Zhang, L. Guo, ACS Nano 13 (2019) 4191–4198.
[116] H. Lin, X.G. Wang, L.D. Yu, Y. Chen, J.L. Shi, Nano Lett. 17 (2017) 384–391.
[117] W.Y. Duan, X.W. Yin, Q. Li, L. Schlier, P. Greil, N. Travitzky, J. Eur. Ceram. Soc. 36 (2016) 3681–3689.
[118] Y. Wang, F. Luo, W.C. Zhou, D.M. Zhu, J. Electron. Mater. 46 (2017) 5225–5231.
[119] J.N. Ma, B. Quan, W. Liu, X.H. Liang, Y.A. Zhang, D.R. Li, Y. Cheng, G.B. Ji, J. Alloys Compd. 709 (2017) 796–801.
[120] B.S. Zhu, Y.M. Tian, Y.K. Wang, L.T. Mao, G. Wen, K.W. Zhang, G.M. Li, Appl. Surf. Sci. 538 (2021), 148018.
[121] C. Zhang, C. Long, S. Yin, R.G. Song, B.H. Zhang, J.W. Zhang, D.P. He, Q. Cheng, Mater. Des. 206 (2021), 109768.
[122] C. Zhang, S. Yin, C. Long, B.W. Dong, D.P. He, Q. Cheng, Opt. Express 29 (2021) 14078–14086.
[123] H.L. Xu, X.W. Yin, M.H. Li, Fang Ye, M.K. Han, Z.X. Hou, X.L. Li, L.T. Zhang, L. F. Cheng, Carbon 132 (2018) 343–351.
[124] Y.P. Dong, X.W. Yin, H.J. Wei, M.H. Li, Z.X. Hou, H.L. Xu, L.F. Cheng, L.T. Zhang, Ceram. Int. 45 (2019) 11316–11324.
[125] B. Wen, M.S. Cao, Z.L. Hou, W.L. Song, L. Zhang, M.M. Lu, H.B. Jin, X.Y. Fang, W. Z. Wang, J. Yuan, Carbon 65 (2013) 124–139.
[126] Y.P. Dong, X.M. Fan, H.J. Wei, Z.X. Hou, M.H. Li, Q. Qu, X.W. Yin, L.F. Cheng, L. T. Zhang, Ceram. Int. 14 (2020) 22474–22481.
[127] J.R. Ma, J.C. Shu, W.Q. Cao, M. Zhang, X.X. Wang, J. Yuan, M.S. Cao, Compos. Part B 166 (2019) 187–195.
[128] H.J. Wei, X.W. Yin, X. Li, M.H. Li, X.L. Dang, L.T. Zhang, L.F. Cheng, Carbon 147 (2019) 276–283.
[129] H.J. Wei, X.W. Yin, Z.X. Hou, F.R. Jiang, H.L. Xu, M.H. Li, L.T. Zhang, L.F. Cheng, J. Eur. Ceram. Soc. 38 (2018) 4189–4197.
[130] H.J. Wei, X.W. Yin, X.L. Dang, L.T. Zhang, L.F. Cheng, Ceram. Int. 44 (2018) 22784–22793.
[131] L. Kong, X.W. Yin, L.T. Zhang, L.F. Cheng, J. Am. Ceram. Soc. 95 (2012) 3158–3165.
[132] Y. Liu, F. Luo, J.B. Su, W.C. Zhou, D.M. Zhu, Phys. Status Solidi A 211 (2014) 2574–2579.
[133] X.L. Li, Z.X. Li, X.G. Liu, S.H. Zhang, S.L. Ran, J. Phys. D 50 (2017), 485302.
[134] G.M. Li, L.T. Mao, B.S. Zhu, X. Chang, Y.K. Wang, G.Z. Wang, K.W. Zhang, Y. M. Tian, L.P. Liang, J. Mater. Chem. C 8 (2020) 14238–14245.
[135] B.S. Zhu, Y.M. Tian, Y.K. Wang, L.T. Mao, F. Gao, G. Wen, L.P. Liang, K.W. Zhang, G.M. Li, ACS Appl. Electron. Mater. 2 (2020) 3307–3319.
[136] K.C. Feng, P.Y. Chen, P.H. Wu, C.S. Chen, C.S. Tu, J. Alloys Compd. 765 (2018) 75–81.
[137] D. Chen, F. Luo, L. Gao, W.C. Zhou, D.M. Zhu, J. Eur. Ceram. Soc. 38 (2018) 4440–4445.
[138] D. Chen, F. Luo, W.C. Zhou, D.M. Zhu, Mater. Lett. 221 (2018), 172–144.
[139] L.A. Zhou, J.L. Huang, X.G. Wang, G.X. Su, J.Y. Qiu, Y.L. Dong, J. Alloys Compd. 774 (2019) 813–819.
[140] Y.C. Qing, W.C. Zhou, F. Luo, D.M. Zhu, Ceram. Int. 43 (2017) 870–874.
[141] L. Zhou, J.L. Huang, H.B. Wang, M. Chen, Y.L. Dong, F.K. Zheng, J. Mater. Sci. 30 (2019) 1896–1906.
[142] Y. Guo, X. Jian, L. Zhang, C.H. Mu, L.J. Yin, J.L. Xie, N. Mahmood, S.X. Dou, R. C. Che, L.J. Deng, Chem. Eng. J. 15 (2019), 122371.
[143] Z.Q. Yang, C. Xu, Y.L. Xia, Z.M. Xiong, R. Soc. Chem. 7 (2020), 200740.
[144] B. Du, J.J. Qian, P. Hu, C. He, M. Cai, X. Wang, A.Z. Shui, J. Am. Ceram. Soc. 103 (2019) 1732–1743.
[145] Y.J. Ma, F. Yang, S.J. Kou, F. Ye, J.M. Xue, X.M. Fan, S.W. Fan, L.F. Cheng, Ceram. Int. 47 (2021) 24393–24402.
[146] Y.J. Jia, M.A.R. Chowdhury, D.J. Zhang, C.Y. Xu, ACS Appl. Mater. Interfaces 11 (2019) 45862–45874.
[147] Y.Z. Hou, W. Yang, C. Zhong, S.S. Wu, Y. Wu, F.B. Liu, X.X. Huang, G.W. Wen, Chem. Eng. J. 378 (2019), 122239.
[148] Y.Z. Hou, B. Xiao, G.W. Yang, Z.Y. Sun, W. Yang, S.S. Wu, X.X. Huang, G.W. Wen, J. Mater. Chem. C 6 (2018) 7661.
[149] C. Chen, S.F. Zeng, X.C. Han, Y.Q. Tan, W.L. Feng, H.H. Shen, S.M. Peng, H. B. Zhang, J. Mater. Sci. Technol. 54 (2020) 223–229.
[150] X.G. Zhao, S. Dong, C.Q. Hong, X.H. Zhang, J.C. Han, J. Colloid Interface Sci. 568 (2020) 106–116.
[151] Z.W. Ren, W.C. Zhou, Y.C. Qing, S.C. Duan, H.J. Pan, Y.Y. Zhou, N. Li, Ceram. Int. 47 (2021) 8478–8485.
[152] B. Du, C. He, J.J. Qian, M. Cai, X. Wang, A.Z. Shui, J. Am. Ceram. Soc. 102 (2019) 7015–7025.
[153] H. Mei, W.Q. Yang, X. Zhao, L. Yao, Y.T. Yao, C. Chen, L.F. Cheng, Mater. Des. 197 (2021), 109271.
[154] Y. Sun, Y.G. Sun, Appl. Sci. 10 (2020) 1924.
[155] D.H. Ding, J. Wang, X.M. Yu, G. Xiao, C. Feng, W.T. Xu, B. Bai, N. Yang, Y.Q. Gao, X. Hou, G.P. He, Ceram. Int. 46 (2019) 5407–5419.
[156] S.F. Zeng, W.L. Feng, S.Y. Peng, Z. Teng, C. Chen, H.B. Zhang, S.M. Peng, RSC Adv. 9 (2019) 30685.
[157] Y.N. Liu, S.F. Zeng, Z. Teng, W.L. Feng, H.B. Zhang, S.M. Peng, Nanoscale Res. Lett. 15 (2020) 28.
[158] D.H. Ding, J. Wang, G.Q. Xiao, Z.P. Li, B. Bai, J.C. Ren, G.P. He, Int. J. Appl. Ceram. Technol. 17 (2020) 734–744.
[159] Y.R. Feng, X. Guo, K. Huang, H. Elsayed, G. Franchin, H.Y. Gong, P. Colombo, J. Eur. Ceram. Soc. (2021), https://doi.org/10.1016/j.jeurceramsoc.2021.06.007.
[160] J.J. Qian, A.Z. Shui, C. He, X. Wang, M. Cai, Y.D. Pu, P. Hu, B. Du, Ceram. Int. 47 (2021) 8004–8013.
[161] D.H. Ding, Z.P. Li, G.Q. Xiao, S.Y. Yang, Mater. Res. Express. 5 (2018), 025039.
[162] Q.C. Meng, Z.H. Li, Y.M. Zhu, D.D. Feng, H.Y. Tan, Mater. Des. 92 (2016) 18–22.
[163] B.Y. Kuang, Y.K. Dou, Z.H. Wang, M.Q. Ning, H.B. Jin, D.Y. Guo, M.S. Cao, X. Y. Fang, Y.J. Zhao, J.B. Li, Appl. Surf. Sci. 445 (2018) 383–390.
[164] Q. Zhang, Y.Z. Gou, H. Wang, K. Jian, Y.F. Wang, Mater. Design 120 (2017) 90–98.
[165] P. Wang, L.F. Cheng, Y.N. Zhang, H. Wu, Y. Hou, W.Y. Yuan, L.X. Zheng, Ceram. Int. 43 (2017) 7424–7435.

[166] H. Gao, F. Luo, Q.L. Wen, S.C. Duan, W.C. Zhou, D.M. Zhu, Ceram. Int. 44 (2018) 6010–6015.
[167] F. Wan, J.H. Yan, H.M. Xu, J. Eur. Ceram. Soc. 38 (2018) 4356–4362.
[168] H.J. Yang, W.Q. Cao, D.Q. Zhang, T.J. Su, H.L. Shi, W.Z. Wang, J. Yuan, M.S. Cao, ACS Appl. Mater. Interfaces 7 (2015) 7073–7077.
[169] X.A. Jian, W. Tian, J.Y. Li, L.J. Deng, Z.W. Zhou, L. Zhang, H.P. Lu, L.J. Yin, N. Mahmood, ACS Appl. Mater. Interfaces 11 (2019) 15869–15880.
[170] Y.S. Huo, K. Zhao, P. Miao, J. Kong, Z.L. Xu, K. Wang, F.P. Li, Y.F. Tang, ACS Sustain. Chem. Eng. 8 (2020) 10490–10501.
[171] H.J. Yang, M.S. Cao, Y. Li, H.L. Shi, Z.L. Hou, X.Y. Fang, H.B. Jin, W.Z. Wang, J. Yuan, Adv. Opt. Mater. 2 (2014) 214–219.
[172] H. Chen, B. Zhao, Z.F. Zhao, H.M. Xiang, F.Z. Dai, J.C. Liu, Y.C. Zhou, J. Mater. Sci. Technol. 47 (2020) 216–222.
[173] S.C. Duan, D.M. Zhu, W.C. Zhou, F. Luo, Q. Chen, J. Mater. Sci. Mater. Electron. 31 (2020) 2634–2642.
[174] Y. Feng, Y.J. Yang, Q.B. Wen, R. Riedel, Z.J. Yu, ACS Appl. Mater. Interfaces 12 (2020) 16912–16921.
[175] A.M. Bu, Y.F. Zhang, Y. Xiang, Y.J. Yang, W.W. Chen, H.W. Cheng, L. Wang, J. Mater. Res. Technol. 9 (2020) 9153–9161.
[176] H. Gao, F. Luo, Q.L. Wen, Y. Hu, Y.C. Qing, J. Mater. Sci. 53 (2018) 15465–15473.
[177] H. Gao, F. Luo, Q.L. Wen, H.Y. Jia, W.C. Zhou, D.M. Zhu, J. Appl. Polym. Sci. 136 (2019) 47097.
[178] C. Gu, C.Q. Guo, X.C. Dong, Z.M. Hu, P.F. Wu, Z.M. Su, Y.X. Lu, B.B. Xu, Z.J. Yu, A.H. Liu, J. Am. Ceram. Soc. 102 (2019) 7098–7107.
[179] Y. Hou, L.F. Cheng, Y.N. Zhang, Y. Yang, C.R. Deng, Z.H. Yang, Q. Chen, X.Q. Du, L.X. Zheng, ACS Appl. Mater. Interfaces 9 (2017) 43072–43080.
[180] Y. Hou, Y.N. Zhang, X.Q. Du, Y. Yang, C.R. Deng, Z.H. Yang, L.X. Zheng, L. F. Cheng, RSC Adv. 8 (2018) 33574.
[181] Q. Li, X.W. Yin, W.Y. Duan, L. Kong, B.L. Hao, F. Ye, J. Alloys Compd. 565 (2013) 66–72.
[182] C.J. Luo, W.Y. Duan, X.W. Yin, J. Kong, J. Phys. Chem. C 120 (2016) 18721–18732.
[183] H. Mei, X. Zhao, S.X. Zhou, D.Y. Han, S.S. Xiao, L.F. Cheng, Chem. Eng. J. 372 (2019) 940–945.
[184] Z. Meng, R. Li, M.Y. Zheng, G.J. Yuan, G.Y. Zhou, J. Guo, X.T. Zhu, G.N. Ren, X. M. Li, Ceram. Int. 45 (2019) 13561–13566.
[185] Z.W. Ren, W.C. Zhou, Y.C. Qing, S.C. Duan, Q.L. Wen, Y.Y. Zhou, Y.Y. Li, J. Mater. Sci. Mater. Electron. (2020) 1–11.
[186] X.L. Lan, Y.B. Li, Z.J. Wang, Chem. Eng. J. 397 (2020), 125250.
[187] T. Han, R.Y. Luo, G.Y. Cui, L.Y. Wang, J. Eur. Ceram. Soc. 39 (2019) 1743–1756.
[188] Y.M. Shi, F. Luo, D.H. Ding, J. Gui, W.C. Zhou, D.M. Zhu, Phys Status Solidi A 210 (2013) 2668–2673.
[189] Y.M. Shi, F. Luo, D.H. Ding, F. Wan, W.C. Zhou, D.M. Zhu, Int. J. Appl. Ceram. Technol. 13 (2016) 17–22.
[190] E. Tan, Y. Kagawa, A.F. Dericioglu, J. Mater. Sci. 44 (2009) 1172–1179.
[191] F. Wan, F. Luo, Y. Mu, Z.Y. Zeng, W.C. Zhou, Ceram. Int. 41 (2015) 9957–9965.
[192] B.W. Wang, H.M. Li, L.M. Xu, J.X. Chen, G.M. He, RSC Adv. 7 (2017) 12126–12132.
[193] P. Wang, L.F. Cheng, Y.N. Zhan, L.T. Zhang, J. Alloys Compd. 716 (2017) 306–320.
[194] Y.C. Wang, Y. Li, H. Luo, Z.C. Li, Z.A. Li, W. Zhou, P. Xiao, J. Alloys Compd. 786 (2019) 409–417.
[195] Q.B. Wen, Y. Feng, Z.J. Yu, D.L. Peng, N. Nicoloso, E. Ionescu, R. Riedel, J. Am. Ceram. Soc. 99 (2016) 2655–2663.
[196] S.S. Xiao, H. Mei, D.Y. Han, L.F. Cheng, Ceram. Int. 45 (2019) 11475–11483.
[197] L.W. Yang, H.T. Liu, M. Zu, J. Am. Ceram. Soc. 101 (2018) 3402–3413.
[198] X.G. Zang, Y.P. Lu, J. Mater. Sci. Mater. Electron. 31 (2020) 2826–2832.
[199] P. Wang, L.F. Cheng, Y.N. Zhang, W.Y. Yuan, H.X. Pan, H. Wu, Compos. Part A Appl. Sci. Manuf. 104 (2018) 68–80.
[200] L.Q. Chen, X.W. Yin, X.M. Fan, M. Chen, X.K. Ma, L.F. Cheng, L.T. Zhang, Carbon 95 (2015) 10–19.
[201] P. Wang, L.F. Cheng, L.T. Zhang, Carbon 125 (2017) 207–220.
[202] J. Zhang, D.Y. Xu, L. Tong, H.C. Qi, D.L. Zhang, C.C. Wang, J. Alloys Compd. 734 (2018) 16–21.
[203] Y.C. Wang, P. Xiao, W. Zhou, H. Luo, Z. Li, W.B. Chen, Y. Li, Ceram. Int. 44 (2018) 3606–3613.
[204] R.B. Wu, Z.H. Yang, M.S. Fu, K. Zhou, J. Alloys Compd. 687 (2016) 833–838.
[205] Z.B. Li, Y.G. Wang, J. Alloys Compd. 709 (2017) 313–321.
[206] M.K. Han, X.W. Yin, Z.X. Hou, C.Q. Song, X.L. Li, L.T. Zhang, L.F. Cheng, ACS Appl. Mater. Interfaces 9 (2017) 11803–11810.
[207] L.X. Chen, J. Zhao, L. Wang, F. Peng, H. Liu, J.X. Zhang, J.W. Gu, Z.H. Guo, Ceram. Int. 45 (2019) 11756–11764.
[208] Z.X. Hou, J.M. Xue, H.J. Wei, X.M. Fan, F. Ye, S.W. Fan, L.F. Cheng, L.T. Zhang, Ceram. Int. 46 (2020) 18160–18167.
[209] M.K. Han, X.W. Yin, W.Y. Duan, S. Ren, L.T. Zhang, L.F. Cheng, J. Eur. Ceram. Soc. 36 (2016) 2695–2703.
[210] Y.Z. Hou, B. Xiao, Z.Y. Sun, W. Yang, S.S. Wu, S. Qi, G.W. Wen, X.X. Huang, Ceram. Int. 45 (2019) 16369–16379.
[211] R.B. Wu, K. Zhou, Z.H. Yang, X.K. Qian, J. Wei, L. Liu, Y.Z. Huang, L.B. Kong, L. Y. Wang, CrystEngComm 15 (2013) 570–576.
[212] F. Wan, F. Luo, H.Y. Wang, Z.B. Huang, W.C. Zhou, D.M. Zhu, Ceram. Int. 40 (2014) 15849–15857.
[213] C.H. Wang, Y.S. Liu, Q.W. You, F. Ye, L.F. Cheng, Ceram. Int. 45 (2019) 5637–5647.
[214] X.L. Ye, Z.F. Chen, J.X. Zhang, C. Wu, Q.B. Zhou, S.F. Ai, H.Z. Liu, S. Cui, Inorg. Chem. Front. 6 (2019) 1579.
[215] X.L. Ye, Z.F. Chen, M. Li, T. Wang, C. Wu, J.X. Zhang, Q.B. Zhou, H.Z. Liu, S. Cui, ACS Sustain. Chem. Eng. 7 (2019) 18395–18404.
[216] Z.J. Yu, X. Lv, K.W. Mao, Y.J. Yang, A.H. Liu, J. Adv. Ceram. 9 (2020) 617–628.
[217] Q. Zhang, C. Zeng, Z. Wu, Z.Y. Xie, Y.H. Zou, D.C. Chen, Mater. Lett. 255 (2019), 126579.
[218] J.M. Zhao, W.X. An, D.A. Li, X.L. Yang, Synth. Met. 161 (2011) 2144–2148.
[219] M.Y. Sun, Q.G. Li, S.F. Huang, X. Cheng, Ceram. Int. 41 (2015) 6084–6088.
[220] H. Luo, Y.Q. Tan, Y. Li, P. Xiao, L.W. Deng, S.F. Zeng, G.J. Zhang, H.B. Zhang, X. S. Zhou, S.M. Peng, J. Eur. Ceram. Soc. 37 (2017) 1961–1968.
[221] C.B. Cheng, R.H. Fan, Z.Y. Wang, P.T. Xie, C.X. Hou, G.H. Fan, Y.H. Lei, L.Q. An, Y. Liu, J. Am. Ceram. Soc. 101 (2018) 1598–1606.
[222] Z.X. Hou, X.W. Yin, H.L. Xu, H.J. Wei, M.H. Li, L.F. Cheng, L.T. Zhang, ACS Appl. Mater. Interfaces 11 (2019) 5364–5372.
[223] X.M. Li, L.T. Zhang, X.W. Yin, J. Eur. Ceram. Soc. 33 (2013) 647–651.
[224] A. Saleem, Y.J. Zhang, H.Y. Gong, M.K. Majeed, X. Lin, J. Jing, M.M. Sheng, C. C. Zhao, J. Mater. Sci. Mater. Electron. 31 (2020) 2918–2925.
[225] W. Zhou, Y. Li, L. Long, H. Luo, Y.C. Wang, J. Am. Ceram. Soc. 103 (2020) 6822–6832.
[226] W. Zhou, L. Long, Y. Li, J. Mater. Sci. Technol. 36 (2019) 55–60.
[227] W.H. Hong, S. Dong, P. Hu, X.G. Luo, S.Y. Du, Ceram. Int. 43 (2017) 14301–14308.
[228] S. Dong, X.H. Zhang, D.Y. Zhang, B.Q. Sun, L.W. Yan, X.G. Luo, J. Eur. Ceram. Soc. 38 (2018) 29–39.
[229] S.S. Xiao, H. Mei, D.Y. Han, L.F. Cheng, Compos. Part B-Eng. 183 (2020), 107629.
[230] M.A. Li, X.W. Yin, G.P. Zheng, M. Chen, M.J. Tao, L.F. Cheng, L.T. Zhang, J. Mater. Sci. 50 (2015) 1478–1487.
[231] X.M. Li, L.T. Zhang, X.W. Yin, L.Y. Feng, Q. Li, Scr. Mater. 63 (2010) 657–660.
[232] X.M. Li, G.J. Yuan, Y.L. Zhou, X.T. Zhu, G.N. Ren, Ceram. Int. 44 (2018) 1176–1181.
[233] M.X. Li, L.F. Cheng, R. Mo, F. Ye, X.W. Yin, J. Alloys Compd. 798 (2019) 280–289.
[234] H. Luo, W.B. Chen, W. Zhou, L. Long, L.W. Deng, Ceram. Int. 43 (2017) 12328–12332.
[235] R. Mo, X.W. Yin, F. Ye, X.F. Liu, X.K. Ma, Q. Li, L.T. Zhang, L.F. Cheng, J. Eur. Ceram. Soc. 39 (2019) 743–754.
[236] P. Wang, L.F. Cheng, Y.N. Zhang, L.T. Zhang, ACS Appl. Mater. Interfaces 9 (2017) 28844–28858.
[237] Z.L. Wen, W. Zhou, L. Long, Y. Li, J. Nanosci. Nanotechnol. 20 (2020) 1859–1865.
[238] J.M. Xue, X.W. Yin, L.F. Cheng, Chem. Eng. J. 378 (2019), 122213.
[239] G.P. Zheng, X.W. Yin, J. Wang, M.L. Guo, X. Wang, J. Mater. Sci. Technol. 28 (2012) 745–750.
[240] G.P. Zheng, X.W. Yin, S.H. Liu, X.M. Liu, J.L. Deng, Q. Li, J. Eur. Ceram. Soc. 33 (2013) 2173–2180.
[241] Q. Zhou, X.W. Yin, F. Ye, R. Mo, X.F. Liu, X.M. Fan, L.F. Cheng, L.T. Zhang, J. Am. Ceram. Soc. 101 (2018) 5552–5563.
[242] W. Zhou, L. Long, G.B. Bu, Y. Li, Adv. Eng. Mater. 21 (2019), 1800665.
[243] W. Zhou, R.M. Yin, L. Long, H. Luo, W.D. Hu, Y.H. Ding, Y. Li, Ceram. Int. 44 (2018) 2249–2254.
[244] Q. Zhou, X.W. Yin, F. Ye, Z.M. Tang, R. Mo, L.F. Cheng, Ceram. Int. 45 (2019) 6514–6522.
[245] Z.X. Cai, L. Su, H.J. Wang, M. Niu, L.T. Tao, D. Lu, L. Xu, M.Z. Li, H.F. Gao, ACS Appl. Mater. Interfaces 13 (2021) 16704–16712.
[246] W. Zhou, R.M. Yin, L. Long, H. Luo, W.D. Hu, Y.H. Ding, Y. Li, Ceram. Int. 44 (2018) 12301–12307.
[247] F. Ye, Q.A. Song, Z.C. Zhang, W. Li, S.Y. Zhang, X.W. Yin, Y.Z. Zhou, H.W. Tao, Y. S. Liu, L.F. Cheng, L.T. Zhang, H.J. Li, Adv. Funct. Mater. 28 (2018), 1707205.
[248] Q. Li, X.W. Yin, L.T. Zhang, L.F. Ceram. Int. 42 (2016) 19237–19244.
[249] Y.Z. Wang, X. Guo, Y.R. Feng, X. Lin, H.Y. Gong, Ceram. Int. 43 (2017) 15551–15555.
[250] Y.R. Feng, X. Guo, H.Y. Gong, Y.J. Zhang, Y. Liu, X. Lin, J.J. Mao, Ceram. Int. 44 (2018) 10420–10425.
[251] Y. Liu, Y.R. Feng, H.Y. Gong, Y.J. Zhang, X. Lin, B.Y. Xie, J.J. Mao, Ceram. Int. 44 (2018) 10945–10950.
[252] Y.R. Feng, X. Guo, H.Y. Gong, Y.J. Zhang, Y. Liu, X. Lin, J.J. Mao, Ceram. Int. 44 (2018) 15686–15689.
[253] C.K. Song, L.F. Cheng, Y.S. Liu, M.X. Zhao, F. Ye, Ceram. Int. 44 (2018) 18759–18769.
[254] C.H. Wang, Y.S. Liu, M.X. Zhao, F. Ye, L.F. Cheng, Ceram. Int. 44 (2018) 22830–22839.
[255] S. Wang, H.Y. Gong, Y.J. Zhang, M.Z. Ashfaq, Ceram. Int. 47 (2021) 1294–1302.
[256] M.X. Zhao, Y.S. Liu, N. Chai, H.L. Qin, X.F. Liu, F. Ye, L.F. Cheng, L.T. Zhang, J. Eur. Ceram. Soc. 38 (2018) 1334–1340.
[257] F. Ye, L.T. Zhang, X.W. Yin, Y.J. Zhang, L. Kong, Y.S. Liu, L.F. Cheng, J. Eur. Ceram. Soc. 34 (2014) 205–215.
[258] X. Guo, Y.R. Feng, X. Lin, Y. Liu, H.Y. Gong, Y.J. Zhang, J. Eur. Ceram. Soc. 38 (2018) 1327–1333.
[259] F.Y. Ren, J.M. Xue, X.L. Liu, L.F. Cheng, Carbon 168 (2020) 278–289.
[260] W. Li, X.C. Li, W. Gong, P.G. Chen, Y.L. Zhu, B.Q. Zhu, Ceram. Int. 46 (2020) 7823–7832.
[261] L.Y. Yang, L.H. Yin, C.Q. Hong, S. Dong, C. Liu, X.H. Zhang, J. Colloid Interface Sci. 582 (2021) 270–282.
[262] C.J. Luo, Y.S. Tang, T. Jiao, J. Kong, ACS Appl. Mater. Interfaces 10 (2018) 28051–28061.
[263] C.J. Luo, T. Jiao, J.W. Gu, Y.S. Tang, J. Kong, ACS Appl. Mater. Interfaces 10 (2018) 39307–39318.
[264] Z.L. Cheng, Y.S. Liu, F. Ye, C.Y. Zhang, H.L. Qin, J. Wang, L.F. Cheng, J. Eur. Ceram. Soc. 40 (2020) 1149–1158.

[265] J.X. Ding, F.B. Chen, J.X. Chen, J. Liang, J. Kong, J. Am. Ceram. Soc. 104 (2021) 1772–1784.
[266] X. Guo, F.F. Xiao, J. Li, H. Zhang, Q.Q. Hu, G.C. Li, H.B. Sun, Ceram. Int. 47 (2021) 1184–1190.
[267] X. Guo, Y.R. Feng, H.B. Sun, Q.Q. Hu, Ceram. Int. 46 (2020) 27634–27640.
[268] Y.Q. He, X.Y. Li, J.X. Zhang, X.G. Li, M.X. Yu, Y.S. Duan, D.L. Jiang, T. Qiu, Int. J. Appl. Ceram. Technol. 15 (2018) 522–530.
[269] Q. Li, X.W. Yin, W.Y. Duan, B.L. Hao, L. Kong, X.M. Liu, J. Eur. Ceram. Soc. 34 (2014) 589–598.
[270] X.M. Liu, Z.J. Yu, L.Q. Chen, B.B. Xu, S. Li, X.W. Yin, R. Riedel, J. Am. Ceram. Soc. 100 (2017) 4649–4660.
[271] X.M. Liu, Z.J. Yu, R. Ishikawa, L.Q. Chen, X.W. Yin, Y.C. Ikuharad, R. Riedel, J. Mater. Chem. C 5 (2017) 7950.
[272] Y. Liu, Y.R. Feng, H.Y. Gong, X. Guo, X. Lin, B.Y. Xie, Y.J. Zhang, J. Mater. Sci. Mater. Electron. 29 (2018) 12496–12502.
[273] Y. Liu, Y.R. Feng, H.Y. Gong, X. Guo, A. Saleem, X. Lin, B.Y. Xie, Y.J. Zhang, J. Eur. Ceram. Soc. 34 (2018) 589–598.
[274] X.L. Liu, J.M. Xue, F. Yang, F. Ye, X.M. Fan, L.F. Cheng, J. Am. Ceram. Soc. 103 (2020) 6255–6264.
[275] Y. Liu, Y.R. Feng, H.Y. Gong, Y.J. Zhang, X. Lin, B.Y. Xie, J.J. Mao, J. Alloys Compd. 749 (2018) 620–627.
[276] Y. Liu, X. Lin, H.Y. Gong, Y.J. Zhang, Y.R. Feng, J.J. Mao, B.Y. Xie, J. Alloys Compd. 771 (2019) 356–363.
[277] X. Long, C.W. Shao, J. Wang, ACS Appl. Mater. Interfaces 11 (2019) 22885–22894.
[278] C.J. Luo, T. Jiao, Y.S. Tang, J. Kong, Adv. Eng. Mater. 20 (2018), 1701168.
[279] H.L. Qin, Y.S. Liu, F. Ye, Z.L. Cheng, C. Chen, L.F. Cheng, L.T. Zhang, J. Alloys Compd. 771 (2018) 747–754.
[280] F.Y. Ren, X.W. Yin, R. Mo, F. Ye, L.T. Zhang, L.F. Cheng, Ceram. Int. 45 (2019) 14238–14248.
[281] C.K. Song, X.F. Liu, F. Ye, Y.S. Liu, L.F. Cheng, J. Eur. Ceram. Soc. 39 (2019) 4417–4423.
[282] S. Wang, X. Lin, M.Z. Ashfaq, X.F. Zhang, C.C. Zhao, M.M. Sheng, R.K. Yang, Y. R. Pei, H.Y. Gong, Y.J. Zhang, J. Mater. Sci. Mater. Electron. 31 (2020) 3803–3816.
[283] P. Wang, L.F. Cheng, L.T. Zhang, Chem. Eng. J. 338 (2018) 248–260.
[284] J.M. Xue, X.W. Yin, H.X. Pan, X.F. Liu, L.T. Zhang, L.F. Cheng, J. Am. Ceram. Soc. 99 (2016) 2672–2679.
[285] J.M. Xue, X.W. Yin, F. Ye, L.T. Zhang, L.F. Cheng, J. Am. Ceram. Soc. 101 (2018) 1201–1210.
[286] W.Y. Yang, W. Wang, C.X. Xie, J. Am. Ceram. Soc. 102 (2019) 1553–1559.
[287] K.X. Hu, H.H. Wang, X. Zhang, H. Huang, T. Qiu, Y. Wang, C.F. (John) Zhang, L. M. Pan, J. Yang, Chem. Eng. J. 408 (2021), 127283.
[288] X. Li, C.Y. Wen, L.T. Yang, R.X. Zhang, X.H. Li, Y.S. Li, R.C. Che, Carbon 175 (2021) 509–518.
[289] Y. Liu, F. Luo, J.B. Su, W.C. Zhou, D.M. Zhu, Z.M. Li, J. Alloys Compd. 619 (2015) 854–860.
[290] H. Gao, F. Luo, H.Y. Nan, Q.L. Wen, Y.C. Qing, C.H. Wang, W.C. Zhou, D.M. Zhu, J. Alloys Compd. 791 (2019) 51–59.
[291] A. Garg, S. Goel, N. Kumari, A. Dubey, N.E. Prasad, S. Tyagi, J. Electron. Mater. 49 (2020) 2233–2241.
[292] B. Ji, S.W. Fan, L. Wang, C.H. Luan, S.J. Kou, J.L. Deng, L.F. Cheng, L.T. Zhang, Ceram. Int. 46 (2020) 22635–22642.
[293] Y. Liu, F. Luo, J.B. Su, W.C. Zhou, D.M. Zhu, J. Electron. Mater. 44 (2015) 867–873.
[294] Y. Liu, F. Luo, Y. Wang, J.B. Su, W.C. Zhou, D.M. Zhu, J. Alloys Compd. 629 (2015) 208–213.
[295] Y. Liu, F. Luo, J.B. Su, W.C. Zhou, D.M. Zhu, J. Alloys Compd. 632 (2015) 623–628.
[296] Y. Liu, Y.Y. Li, F. Luo, X.L. Su, J. Xu, J.B. Wang, X.H. He, Y.H. Qu, J. Alloys Compd. 715 (2017) 21–28.
[297] Y. Liu, X.Y. Jian, X.L. Su, F. Luo, J. Xu, J.B. Wang, X.H. He, Y.H. Qu, J. Alloys Compd. 740 (2018) 68–76.
[298] J.B. Su, W.C. Zhou, Y. Liu, Y.C. Qing, F. Luo, D.M. Zhu, J. Mater. Sci. Mater. Electron. 27 (2016) 2460–2466.
[299] Q.L. Wen, W.C. Zhou, Y.D. Wang, Y.C. Qing, F. Luo, D.M. Zhu, Z.B. Huang, J. Mater. Sci. 52 (2017) 832–842.
[300] D. Zhao, S.Q. Xia, Y.G. Wang, M.D. Wang, Appl. Phys. A 126 (2020) 1–9.
[301] L.Y. Liang, Q.M. Li, X. Yan, Y.Z. Feng, Y.M. Wang, H.-B. Zhang, X.P. Zhou, C. T. Liu, C.Y. Shen, X.L. Xie, ACS Nano 15 (2021) 6622–6632.
[302] J.C. Shu, W.Q. Cao, M.S. Cao, Adv. Funct. Mater. 31 (2021), 2100470.
[303] R. Kumar, S. Sahoo, E. Joanni, R.K. Singh, W.K. Tan, K.K. Kar, A. Matsuda, Carbon 177 (2021) 304–331.
[304] Y. Bhattacharjee, S. Bose, ACS Appl. Nano Mater. 4 (2021) 949–972.
[305] Z.W. Zhang, Z.H. Cai, Z.Y. Wang, Y.L. Peng, L. Xia, S.P. Ma, Z.Z. Yin, Y. Huang, Nano-Micro Lett. 13 (2021) 56.
[306] T.T. Li, L. Xia, H. Yang, X.Y. Wang, T. Zhang, X.X. Huang, L. Xiong, C.L. Qin, G. W. Wen, ACS Appl. Mater. Interfaces 13 (2021) 11911–11919.
[307] H.K. Choi, A. Lee, M. Park, D.S. Lee, S. Bae, S.K. Lee, S.H. Lee, T. Lee, T.W. Kim, ACS Nano 15 (2021) 829–839.
[308] X. Li, M.H. Li, X.K. Lu, W.J. Zhu, H.L. Xu, J.M. Xue, F. Ye, Y.S. Liu, X.M. Fan, L. F. Cheng, Chem. Eng. J. 419 (2021), 129414.
[309] Y. Wang, Z.W. Fan, H. Zhang, J. Guo, D.X. Yan, S.F. Wang, K. Dai, Z.M. Li, Mater. Des. 197 (2021), 109222.
[310] X.J. Zeng, Y. Zhao, X.D. Hu, G.D. Stucky, M. Moskovits, Small Struct. 2 (2021), 2000138.
[311] X.J. Zeng, H.B. Song, Z.Y. Shen, M. Moskovits, J. Materiomics (2021), https://doi.org/10.1016/j.jmat.2021.03.001.
[312] Y.C. Qing, H.Y. Yao, Y. Li, F. Luo, J. Eur. Ceram. Soc. 41 (2021) 1071–1075.
[313] Y. Hou, L.F. Cheng, Y.N. Zhang, X.Q. Du, Y.J. Zhao, Z.H. Yang, Chem. Eng. J. 404 (2021), 126521.
[314] J.Q. Tao, J.T. Zhou, Z.J. Yao, Z.B. Jiao, B. Wei, R.Y. Tan, Z. Li, Carbon 172 (2021) 542–555.
[315] Y.C. Wang, W. Zhou, G.L. Zeng, H. Chen, H. Luo, X.M. Fan, Y. Li, Carbon 175 (2021) 233–242.
[316] Y. Li, B. Xue, S.D. Yang, Z.L. Cheng, L. Xie, Q. Zheng, Chem. Eng. J. 410 (2021), 128356.
[317] M.T. Qiao, J.X. Li, D. Wei, X.W. He, X.F. Lei, J. Wei, Q.Y. Zhang, Microporous Mesoporous Mater. 314 (2021), 110867.
[318] J.C. Dong, M. Su, V. Briega-Martos, L. Li, J.B. Le, P. Radjenovic, X.S. Zhou, J. M. Feliu, Z.Q. Tian, J.F. Li, DJ, Am. Chem. Soc. 142 (2020) 715–719.
[319] X.D. Li, S.M. Wang, L. Li, Y.F. Sun, Y. Xie, J. Am. Chem. Soc. 142 (2020) 9567–9581.
[320] J.Z. Chen, G.G. Liu, Y.Z. Zhu, M. Su, P.F. Yin, X.J. Wu, Q.P. Lu, C.L. Tan, M. T. Zhao, Z.Q. Liu, W.M. Yang, H. Li, G.H. Nam, L.P. Zhang, Z.H. Chen, X. Huang, P.M. Radjenovic, W. Huang, Z.Q. Tian, J.F. Li, H. Zhang, J. Am. Chem. Soc. 142 (2020) 7161–7167.
[321] S.Y. Wu, M.R. Li, Y.G. Sun, Angew. Chem. Int. Ed. 58 (2019) 8987–8995.
[322] G. Malta, S.A. Kondrat, S.J. Freakley, C.J. Davies, L. Lu, S. Dawson, A. Thetford, E. K. Gibson, D.J. Morgan, W. Jones, P.P. Wells, P. Johnston, C.R.A. Catlow, C. J. Kiely, G.J. Hutchings, Science 355 (2017) 1399–1403.
[323] J.C. Shu, M.S. Cao, M. Zhang, X.X. Wang, W.Q. Cao, X.Y. Fang, M.Q. Cao, Adv. Funct. Mater. 30 (2020), 1908299.
[324] Z.B. Pan, L.M. Yao, J.W. Zhai, X. Yao, H. Chen, Adv. Mater. 30 (2018), 1705662.
[325] J.C. Shu, X.Y. Yang, X.R. Zhang, X.Y. Huang, M.S. Cao, L. Li, H.J. Yang, W.W. Cao, Carbon 162 (2020) 157–171.